AD-A066 199 RENSSELAER POLYTECHNIC INST TROY N Y DEPT OF MATHEMA--ETC F/G 8/10
ANALYSIS OF ACOUSTICAL EFFECTS OF RECEIVER AND SOURCE MOTIONS A--ETC(U)
MAR 79 M J JACOBSON, W L SIEGMANN, J L KAYS N00014-76-C-0288

UNCLASSIFIED RPI-MATH-124 NL

| OF |
AD
AD66199

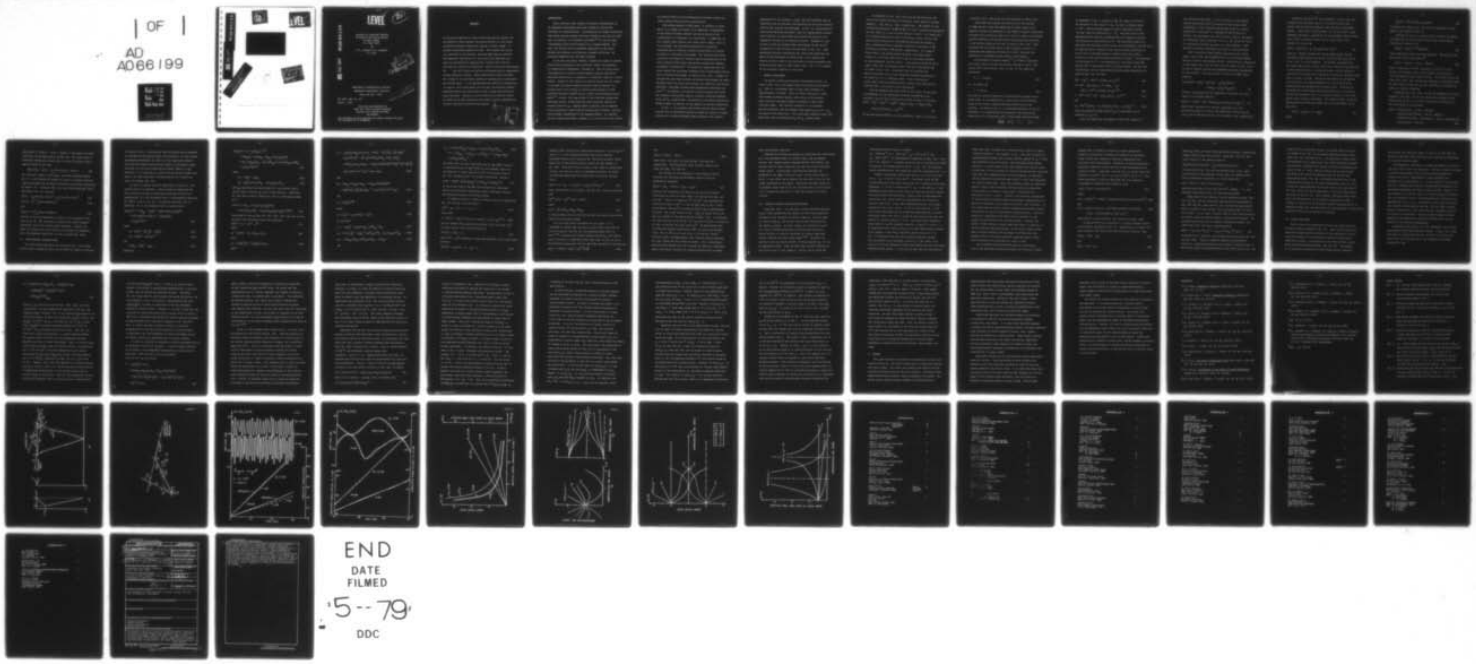

END
DATE
FILMED
5--79
DDC

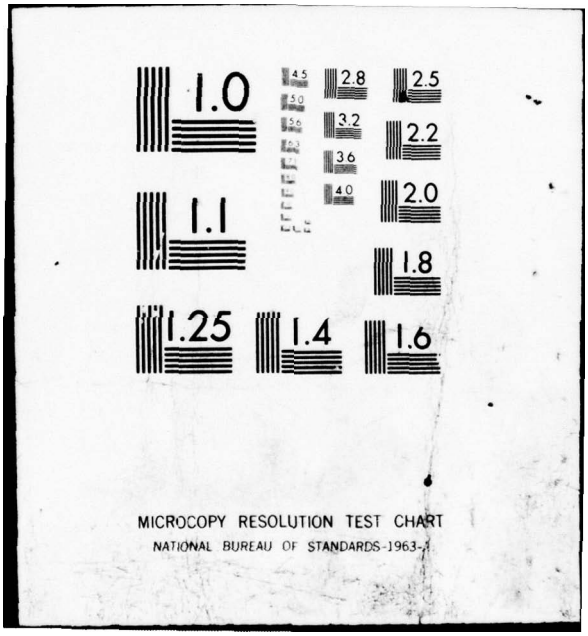
1.0
1.1
1.25
1.4
1.6
1.8
2.0
2.2
2.5
2.8
3.2
3.6
4.0
4.5
5.0
5.6
MICROCOPY RESOLUTION TEST CHART
NATIONAL BUREAU OF STANDARDS-1963-A

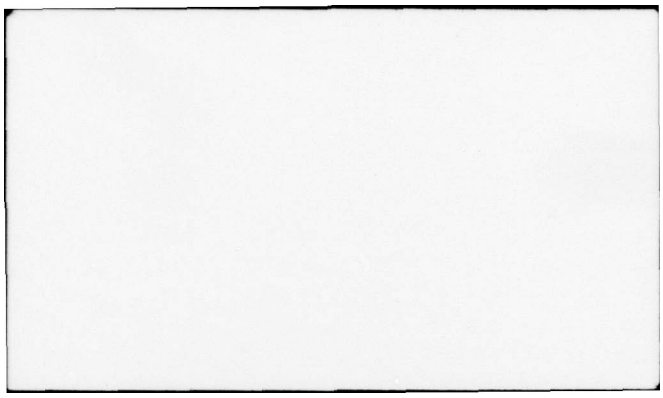

Analysis of Acoustical Effects of Receiver and Source Motions at Short Ranges in a Deep Ocean

by

M.J. Jacobson, W.L. Siegmann,
J.L. Kays

Department of Mathematical Sciences
Rensselaer Polytechnic Institute
Troy, New York 12181

RPI Math. Rep. No. 124

March 1, 1979

This work was sponsored by
Code 222, Office of Naval Research
Contract No. N 00014-76-C-0288
NR 386-606

ABSTRACT

An analytical approach is used to determine general results for the effects of both receiver and source motions on a CW signal transmitted through a deep ocean channel at short ranges. A bilinear sound-speed profile is used. The receiver and source are restricted to the surface, and only SRBR rays are relevant. Time-dependent expressions for the total-field amplitude and phase are developed for appropriately limited time intervals, and numerical results are presented. General analytical expressions for the total field are derived and demonstrated to approximate closely numerical results. These expressions provide the basis for a study of the acoustical effects of varying motion parameters and initial range. It is demonstrated that effects of differences in range on total-field phase rate and the time interval between amplitude maxima are significant at short ranges and diminish as range increases. Effects on total-field due to receiver motion are shown to be both significant and widely varying, depending on receiver and source directions and speeds.

INTRODUCTION

Until recently, most studies of acoustic transmissions in an underwater environment have been limited to sources and receivers in fixed positions. Investigations of energy transmitted from moving sources usually have been limited to the area of radar and, in acoustics, to classical treatments[1,2] of line-of-sight transmissions from sources moving in an isospeed medium. However, the results are not generally applicable in the ocean, because such effects as refraction, boundary reflection, and multipath summation have not been included.

In the past few years, however, studies have begun to address moving-source problems in more realistic oceanic environments, as exemplified by References 3 through 10. Most of these recent investigations of relative motion between receiver and source have been restricted to a receiver, or receivers, fixed in a static medium. Studies of the effects of receiver motion are not common in the open literature despite practical uses including a co-located source and receiver in active moving systems to form synthetic aperture arrays[10] and to conduct echo-sounding measurements.[11] In part, this may be due to the classical discussions mentioned earlier, which show that some acoustical effects of receiver motion (e.g., Doppler-shift frequency) can be deduced from an equivalent fixed receiver-moving source problem, assuming line-of-sight transmission in an isospeed medium. For dynamic and more complicated media, however, it is not correct that effects

of receiver motion can be determined by extending results of fixed receiver-moving source investigations.

The primary purpose of this paper, in contrast to those above, is to apply ray theory in an analytical investigation of the effects of both receiver and source motion on the transmission of a CW signal in a deep ocean. In addition, we will examine these effects over rather short ranges, since to our knowledge, the literature pertaining to acoustical investigations of relative receiver-source motion is limited virtually to relatively long ranges. Our analysis will permit a specific description of receiver-motion contributions to the total acoustic field, which necessarily include both temporal and spatial fluctuations.[4] We assume for simplicity that the ocean channel has horizontal boundaries and a sound-speed profile that is bilinear with depth, as shown in Fig. 1(a). Further, we consider the case where surface and bottom sound speeds are equal, and where both the source and receiver are located at the surface. Therefore, only SRBR (surface-reflected/bottom-reflected) rays exist.[12] In addition, the motions of both receiver and source are limited to horizontal paths at constant velocities denoted by $\vec{v}_1$ and $\vec{v}_2$, respectively. Relaxation of the above restrictions could be made, if desired, at the expense of relative simplicity.

In Sec. I, we transform the moving receiver-moving source problem into an equivalent problem in which all motion is viewed relative to a moving reference frame located on the receiver.

Expressions for the geometry, travel time and spreading loss of individual rays are derived, and equations for the total acoustic field at the receiver are developed. In Sec. II, expressions for total-field amplitude and phase, valid for appropriately limited time intervals, are determined and provide the basis for the subsequent calculation of numerical results. Examples of such results at both the minimum (2km) and maximum (10 km) of the assumed short-range interval are presented in Sec. III. Then, approximate analytic expressions for total-field amplitude and phase are derived which are used in Sec. IV to explain the effects on total-field of the variation of motion parameters and receiver-source range at some initial time. Sec. V is a summary of the principal findings in this paper.

I. GENERAL DEVELOPMENT

We assume a deep-ocean bilinear sound-speed profile, as shown in Fig. 1(a), with equal bottom and surface sound speeds c_b. This is a reasonable model in many ocean channels of approximately 5 km depth. Also, we choose initially a fixed, left-handed coordinate system, with origin at the surface, where asterisks designate spatial variables in this fixed reference frame. The vertical coordinate z* is measured positive downward, and the minimum sound speed c_m is at $z^* = h_m$, the depth of the SOFAR axis. The sound-speed gradients above and below this axis are denoted by g_1 and g_2, respectively.

As suggested in Fig. 1(b), both receiver $\mathcal{R}$ and source $\mathcal{S}$ are on the surface and move on horizontal linear paths at constant speeds $v_1 = |\vec{v}_1|$ and $v_2 = |\vec{v}_2|$, respectively. The symbols O' and O denote the positions of $\mathcal{R}$ and $\mathcal{S}$ at a time $\hat{t}$ arbitrarily designated as zero, while R_o is the distance between O' and O. For simplicity, y^* is measured positive in the O'O direction, while receiver and source path directions are described by defining the angles λ_o and γ_o measured positive clockwise from the y^* direction to the directions of motion of $\mathcal{R}$ and $\mathcal{S}$, respectively. At a generic source time $\hat{t}$, the moving source $\mathcal{S}$ emits a CW signal which travels in a vertical plane and arrives at the moving receiver at some subsequent receiver time t. The positions of $\mathcal{R}$ and $\mathcal{S}$ at times $\hat{t}$ and t for a particular time $\hat{t}$ and for a particular ray are shown in Fig. 1(b). Consistent with our notation for spatial variables, we will use asterisks to denote functions in the fixed x^*, y^*, z^* reference frame. Also, functions of source time $\hat{t}$ will be annotated with a caret, while functions of receiver time t will have no such superscript.

From the geometry and fixed frame of Fig. 1(b), we can write an expression for the horizontal distance traveled by a ray emitted at source time $\hat{t}$ and arriving at $\mathcal{R}$ at time t as follows:

$$\hat{R}^*(\hat{t}) = \{R_o^2 + (v_1 t)^2 + (v_2 \hat{t})^2 - 2R_o v_1 t \cos\lambda_o + 2 R_o v_2 \hat{t} \cos\gamma_o - 2(v_1 t)(v_2 \hat{t})\cos(\lambda_o - \gamma_o)\}^{1/2} . \quad (1)$$

We use the notation $\hat{R}^*(\hat{t})$, in lieu of $\hat{R}^*(\hat{t},t)$, since t is in fact

a function of $\hat{t}$. This point will be discussed in detail soon.

Since both the receiver and source are on the surface, an SRBR ray will cross the SOFAR axis 2N times, where N is a positive integer corresponding to the number of bottom reflections. We denote the inclination angle of a ray by θ, where θ is measured positive downward from the horizontal source-receiver direction in the vertical plane of the ray, as shown in Fig. 1(b). Also, we denote the ray launch angle at $\mathscr{S}$ by $\theta_b(N,\hat{t})$, since θ is completely described by the values of N and $\hat{t}$ and where the subscript b corresponds to the surface sound speed c_b.

As discussed in previous papers,[5,6] if $\hat{T}^*(N,\hat{t})$ represents the travel time of the Nth ray emitted from $\mathscr{S}$ at time $\hat{t}$, then source time $\hat{t}$ and receiver time t in Eq. (1) are implicitly related by

$$\hat{t} = t - \hat{T}^*(N,\hat{t}) \tag{2a}$$

or, in theory, by

$$\hat{t} = F^*(N,t) \ . \tag{2b}$$

To reach our initial objective of obtaining the acoustic total-field at $\mathscr{R}$, it is appropriate to replace the fixed reference frame x*,y*,z* with a moving reference frame x,y,z at the receiver. As shown in Fig. 2, y is measured positive in the O'O direction, z is measured positive downward, and the positive direction of x is consistent with a left-handed reference frame.

As suggested in Fig. 2, relative to $\mathcal{R}$, $\mathcal{L}$ appears to move in the direction of the vector $\vec{v} = \vec{v}_2 - \vec{v}_1$ with a constant speed $v = |\vec{v}|$, and the medium appears to have a spatially uniform "current" which we denote by $\vec{v}_c = -\vec{v}_1$. The path of $\mathcal{L}$ is now described by the angle ψ_o, measured positive clockwise from the O'O direction to the direction of $\vec{v}$. The horizontal angle $\lambda(\hat{t})$ describes the direction of the current (or equivalently, the direction of receiver motion relative to the receiver-source direction at time $\hat{t}$) and is measured positive clockwise from the current direction to the receiver-source direction at time $\hat{t}$. The direction of the current at $\hat{t} = 0$ is denoted by λ_o, horizontal range $\hat{R}(\hat{t})$ and $\cos \lambda(\hat{t})$ at any source time $\hat{t}$ are given by Eqs. (3a) and (3b), respectively, and the relationships between model parameters are given by Eqs. (3c) and (3d):

$$\hat{R}(\hat{t}) = [R_o^2 + (v\hat{t})^2 + 2(v\hat{t})R_o \cos \psi_o]^{1/2} , \tag{3a}$$

$$\cos \lambda(\hat{t}) = [R_o \cos \lambda_o + v\hat{t} \cos(\psi_o - \lambda_o)] \times [R_o^2 + (v\hat{t})^2 + 2(v\hat{t})R_o \cos \psi_o]^{-1/2} , \tag{3b}$$

$$v = |\vec{v}| = [v_1^2 + v_2^2 - 2v_1v_2 \cos(\lambda_o - \gamma_o)]^{1/2} , \tag{3c}$$

and

$$\psi_o = \tan^{-1}[v_2 \sin\gamma_o - v_1 \sin\lambda_o][v_2 \cos\gamma_o - v_1 \cos\lambda_o]^{-1} , \tag{3d}$$

where the multiple-valued function ψ_o is restricted to the interval $0 \leq \psi_o < 2\pi$.

Since the medium may now appear to move with respect to

the reference frame at $\mathcal{R}$, it will be useful to distinguish between expressions valid for moving and stationary media. Accordingly, we will identify expressions valid in a static medium with a subscript "s" (although $\mathcal{R}$ and $\mathcal{S}$ may be in motion), and expressions for which receiver, source, and medium are motionless with a subscript "o" (i.e., $\mathcal{R}$ and $\mathcal{S}$ are fixed at a horizontal distance R_o apart in a still medium). Thus, expressions without subscripts are valid in a moving medium.

Ref. 12 contains rather general expressions for launch angle, travel time, and spreading loss in a stationary medium having a bilinear sound-speed profile. With the prior assumptions in this paper, Eqs. (3a) and (3b) and the results of Ref. 12 can be used to deduce required time-dependent equations appropriate to this problem. The launch angle of one of our SRBR rays is given by

$$\tan \theta_b(N,\hat{t}) = N(g_1^{-1} + g_2^{-1})(c_b^{\,2} - c_m^{\,2})c_b^{-1}[\hat{R}(\hat{t})]^{-1} - [4N(g_1 + g_2)c_b]^{-1} g_1 g_2 \hat{R}(\hat{t}) \ . \qquad (4)$$

Further, the appropriate time-dependent expression for travel time in a stationary medium is

$$T_s(N,t) = 2N(g_1^{-1} + g_2^{-1}) \log[(c_b/c_m)(1+\sin\theta_m)(1+\sin\theta_b)^{-1}], \qquad (5)$$

where "log" represents the natural logarithm, θ_m is the inclination angle of a ray at the SOFAR axis, and $\sin \theta_b$ and $\sin \theta_m$ can be derived from Eq. (4) and Snell's law, respectively.

Extensive analyses[13,14] of ray geometry, travel time, and spreading loss have been made for a uniformly-moving ocean channel with horizontal boundaries and a bilinear sound-speed profile. Using these results and Eq. (5), we can write a time-dependent expression, appropriate for this problem, which relates travel time in a moving channel to the travel time in the absence of a current by

$$\hat{T}(N,\hat{t}) = \hat{T}_s(N,\hat{t})[1 + M_c \cos\theta_b(N,\hat{t})\cos\lambda(\hat{t})]^{-1} , \qquad (6)$$

where $M_c = |\vec{v}_c|c_b^{-1}$ and both the launch angle $\theta_b(N,\hat{t})$ and the horizontal angle between the current direction and the plane of a ray, $\lambda(\hat{t})$, are time-dependent. To consider spreading loss, we assume that a point source, moving with velocity $\vec{v}$ and emitting a unity-amplitude omnidirectional CW signal, travels through a uniform-current medium with velocity $\vec{v}_c$ in which an omnidirectional point receiver is fixed. Neglecting the effects of attenuation and scattering, the amplitude $\hat{A}(N,\hat{t})$ of a ray at $\mathcal{R}$ will be affected only by spreading and boundary losses. Reference 15 developed the relationship between spreading loss in a uniform current and spreading loss in a stationary medium, if the sound speed varies linearly with depth. The results of Ref. 15 may be applied above and below the SOFAR axis of this problem, and we may write

$$\hat{L}(N,\hat{t}) = \hat{L}_S(N,\hat{t})\ [1 + O(M_c)] , \qquad (7a)$$

where

$$\hat{L}_S(N,\hat{t}) = \hat{R}^2(\hat{t})\,\tan^2\theta_b\,\csc\theta_b\csc\theta_m \qquad (7b)$$

is obtained by applying Eq. (3a) and the assumptions of this paper to the results of Ref. 12.

Denoting the loss at a single bottom reflection by $\hat{B}(N,\hat{t})$, the amplitude at the receiver of the arrival with N bottom reflections is taken to be

$$\hat{A}(N,\hat{t}) = [\hat{L}(N,\hat{t})]^{-1/2}[\hat{B}(N,\hat{t})]^N \ , \qquad (8a)$$

since scattering losses are being neglected. The phase of the Nth arrival can be expressed as[12]

$$\hat{\phi}(N,\hat{t}) = \omega\hat{T}(N,\hat{t}) - (N-1)\pi - N\hat{S}(N,\hat{t}) \ , \qquad (8b)$$

where ω represents circular frequency in rad $\sec^{-1}$ at the source, and frequency shift due to Doppler is contained in the time-dependent phase terms $\omega\hat{T}$ and $\hat{S}$. The second term on the right side of Eq. (8b) follows from assuming a π-rad phase shift at each surface reflection, and the term $\hat{S}(N,\hat{t})$ represents the shift at a bottom reflection.

Combining Eqs. (2a), (2b), (4)-(8) and dropping the asterisk notation, since Eqs. (4)-(8) are written with respect to the moving frame at $\mathcal{A}$, we can write the Nth-ray contribution to the total field at the receiver:

$$\begin{aligned} V(N,t) &= \hat{A}(N,\hat{t})\sin[\omega\hat{t} - (N-1)\pi - N\hat{S}(N,\hat{t})] \\ &= \hat{A}(N,\hat{t})\sin\{\omega[t-\hat{T}(N,\hat{t})] - (N-1)\pi - N\hat{S}(N,\hat{t})\} \\ &= A(N,F(N,t))\sin\{\omega t - \omega T[N,F(N,t)] - (N-1)\pi - NS[N,F(N,t)]\} \\ &= A(N,t)\sin[\omega t - \phi(N,t)] \ , \end{aligned} \qquad (9a)$$

where $\phi(N,t) = \omega T(N,t) - (N-1)\pi - NS(N,t)$ is the phase in radians and $A(N,t)$ is the amplitude of the Nth ray. The total field is formed by summing the arrivals and, in terms of receiver time t, may be written in the form

$$\mathcal{A}(t)\sin[\omega t - \Phi(t)] = \sum_N A(N,t)\sin[\omega t - \phi(N,t)] \ . \qquad (9b)$$

For the short ranges in this paper, the above summation begins at N = 1, and although the number of terms is countably infinite, rapid convergence due to bottom reflection loss permits termination at some N = N'. Using Eq. (9b), the total-field amplitude, $\mathcal{A}(t)$, and phase, $\Phi(t)$, are given by:

$$\mathcal{A}^2(t) = [\sum_N A(N,t)\sin\ (N,t)]^2 + [\sum_N A(N,t)\cos\ (N,t)]^2 \ , \qquad (10)$$

$$\sin\Phi(t) = \mathcal{A}^{-1} \sum_N A(N,t)\sin\phi(N,t) \ , \qquad (11a)$$

and

$$\cos\Phi(t) = \mathcal{A}^{-1}\sum_N A(N,t)\ \cos\phi(N,t) \ . \qquad (11b)$$

Because of the time dependence of $\phi(N,t)$ in the argument of the sine terms, Eq. (9b) represents a signal with slight frequency spreading, and is not exactly single frequency. However, we elect to interpret the total field as a CW signal of frequency ω, with time-dependent phase $\Phi(t)$, as well as amplitude $\mathcal{A}(t)$.

II. TIME-DEPENDENT APPROXIMATIONS

The total-field expressions at the end of Sec. I are formal at this point, because $\mathcal{A}$ and Φ are not known as explicit functions

of receiver time t. Fortunately, this difficulty may be overcome by considering sufficiently small time intervals. In the ensuing approximate development, we wish to retain only those effects of source and receiver motion which result in corrections larger than O(M) to total-field amplitude and phase, where $M = vc_b^{-1}$. Therefore, it is necessary to retain only corrections larger than O(M) to the amplitude A(N,t) and phase $\phi(N,t)$ of a single ray (see, for example, Ref. 16).

In order to express α and Φ explicitly in terms of t, the quantity F(N,t) is required. Since an explicit expression for F(N,t) generally cannot be obtained, we proceed to derive an approximation to it by developing first a time-dependent expansion for $\hat{T}(N,\hat{t})$, given in Eq. (6). We begin by using Eq. (3a) to expand Eq. (4) to second-degree terms in source time $\hat{t}$:

$$\tan\theta_b(N,\hat{t}) \doteq \tan\theta_{bo} - (D_1R_o^{-1} + D_2R_o)(\cos\psi_o)(c_b/R_o)M\hat{t}$$
$$+ (1/2)\{D_1R_o^{-1}(3\cos^2\psi_o - 1) + D_2R_o\cos^2\psi_o\}$$
$$\times (c_b/R_o)^2(M\hat{t})^2 , \qquad (12)$$

where

$$D_1 = N(g_1^{-1} + g_2^{-1})(c_b^2 - c_m^2)c_b^{-1} , \qquad (13a)$$

$$D_2 = [4N(g_1^{-1} + g_2^{-1})c_b]^{-1} , \qquad (13b)$$

and

$$\tan\theta_{bo} = D_1R_o^{-1} - D_2R_o . \qquad (13c)$$

Similarly,

$$\cos\theta_b(\hat{t}) = [1 + \tan^2\theta_b(\hat{t})]^{-1/2}$$

$$\doteq \cos\theta_{bo}\Big(1 + E_1 \sin\theta_{bo}\cos\theta_{bo}\cos\psi_o(c_b/R_o)M\hat{t}$$

$$+ \{E_2 \sin\theta_{bo}\cos\theta_{bo} - E_1^2\cos^2\theta_{bo}[1-(3/2)\cos^2\theta_{bo}]\cos^2\psi_o\}$$

$$\times (c_b/R_o)^2(M\hat{t})^2\Big) , \qquad (14)$$

where

$$E_1 = [D_1 R_o^{-1} + D_2 R_o] , \qquad (15a)$$

$$E_2 = D_1 R_o^{-1}[(3/2)\cos^2\psi_o - (1/2)D_2 R_o \sin^2\psi_o , \qquad (15b)$$

and θ_{bo} represents the launch angle of a ray emitted from a source fixed a distance R_o from a fixed receiver. Similarly, Eq. (3b) may be used to expand $\cos\lambda(\hat{t})$ to second-degree terms in $\hat{t}$:

$$\cos\lambda(\hat{t}) \doteq \cos\lambda_o + \sin\lambda_o\sin\psi_o(c_b R_o^{-1})M\hat{t} -$$

$$[(1/2)\cos\lambda_o\sin^2\psi_o + \sin\lambda_o\sin\psi_o\cos\psi_o](c_b R_o^{-1})^2(M\hat{t})^2 . \qquad (16)$$

Using Snell's law and Eqs. (5), (6), (12), (14), and (16), we can now write the following travel-time expansion:

$$\hat{T}(N,\hat{t}) \doteq \alpha_1 + \alpha_2\hat{t} + \alpha_3\hat{t}^2 , \qquad (17)$$

where

$$\alpha_1 = T_o(N)[1 - M_c\cos\theta_{bo}\cos\lambda_o] . \qquad (18)$$

Also,

$$\alpha_2 = G_1 c_b R_o^{-1} M_c M + G_2 c_b R_o^{-1} M\cos\psi_o , \qquad (19a)$$

where

$$G_1 = - T_o(N)\Big(\cos\theta_{bo}\sin\lambda_o\sin\psi_o + \{N(g_1^{-1} + g_2^{-1})(c_b^2 - c_m^2)(c_bR_o)^{-1}$$

$$+ R_o/[(4N)(g_1^{-1} + g_2^{-1})c_b]\}\cos^2\theta_{bo}\sin\theta_{bo}\cos\lambda_o\cos\psi_o\Big)$$

$$- \cos^2\theta_{bo}\csc\theta_{mo}(\sin\theta_{mo} - \sin\theta_{bo})[2N(g_1^{-1}+g_2^{-1})]\{N(g_1^{-1}+g_2^{-1})(c_b^2-c_m^2)$$

$$+ R_o/[(4N)(g^{-1}+g^{-1})c_b]\}\cos\lambda_o\cos\psi_o \qquad (19b)$$

and

$$G_2 = \cos\theta_{bo}\csc\theta_{mo}(\sin\theta_{mo} - \sin\theta_{bo})\{2N(g_1^{-1}+g_2^{-1})\}$$

$$\times \{N(g_1^{-1}+g_2^{-1})(c_b^2-c_m^2)(c_bR_o)^{-1} + R_o/[(4N)(g^{-1}+g^{-1})c_b]\}\ , \qquad (19c)$$

and

$$\alpha_3 \doteq H(c_bR_o^{-1})^2M^2\ , \qquad (20a)$$

where

$$H = [J_2I_1^2 + J_1I_2][2N(g_1^{-1} + g_2^{-1})]\ . \qquad (20b)$$

In the above,

$$I_1 = - (D_1R_o^{-1} + D_2R_o)\cot\theta_{bo}\cos^2\theta_{bo}\cos\psi_o\ , \qquad (20c)$$

$$I_2 = (3/2)(D_1R_o^{-1} + D_2R_o)^2\cos^4\theta_{bo}\cos^2\psi_o + E_2\cot\theta_{bo}\cos^2\theta_{bo}, \qquad (20d)$$

$$J_1 = - \sin\theta_{bo}\csc\theta_{mo}\sec^2\theta_{bo}(\sin\theta_{mo} - \sin\theta_{bo})\ , \qquad (20e)$$

and

$$J_2 = [-(1/2)\sin^4\theta_{bo}(1-\sin\theta_{mo}) + (1/2)\sin^2\theta_{bo}\sin^2\theta_{mo} \quad (20f)$$
$$\times (1 + \sin\theta_{mo} - 2\sin\theta_{bo} + 2\sin^2\theta_{bo}) - 2\sin\theta_{bo}\sin\theta_{mo}]$$
$$\times [\sin^3\theta_{mo}\cos^4\theta_{bo}]^{-1} .$$

We remark that the exact expression for α_3 (Eq.(20a)) contains a term proportional to $M_c M^2$ which we have dropped, since its contribution is small compared to that of the other terms in Eq. (17), assuming that $\hat{t}$ is suitably restricted. Further,

$$T_o(N) = 2N(g_1^{-1} + g_2^{-1})\log[c_b c_m^{-1}(1+\sin\theta_{mo})(1+\sin\theta_{bo})^{-1}] \quad (21)$$

is the travel time of the Nth ray emitted from a stationary source at a horizontal distance R_o from a stationary receiver and traveling through a motionless medium.

To express results in terms of receiver time t, we substitute Eq. (17) into Eq. (2a) and obtain

$$\alpha_3\hat{t}^2 + (\alpha_2 + 1)\hat{t} - (t - \alpha_1) = 0 , \quad (22a)$$

from which

$$\hat{t} = F(N,\hat{t}) = (2\alpha_3)^{-1}\{-(1+\alpha_2) \pm [(1+\alpha_2)^2 + 4\alpha_3(t-\alpha_1)]^{1/2}\}. \quad (22b)$$

We have demonstrated numerically that, for $\hat{t}$ not too large, $\alpha_3\hat{t}^2$ is small and Eq. (22a) may be written as

$$\hat{\tau}(N,\hat{t}) + \hat{\varepsilon}(\hat{t}) = 0 , \quad (22c)$$

where $\hat{\varepsilon}(\hat{t}) = \alpha_3\hat{t}^2$ represents a small perturbation to the unperturbed quantity

$$\hat{\tau}(N,\hat{t}) = (\alpha_2+1)\hat{t} - (t - \alpha_1) = 0 . \quad (22d)$$

Equation (22d) provides the unperturbed solution $\hat{t} = (t-\alpha_1)(\alpha_2+1)^{-1}$. Since $\hat{\varepsilon} << 1$, the difference between this result and the perturbed solution for $\hat{t}$ given by Eq. (22b) must be small, which holds only if the positive sign is chosen for the radical in Eq. (22b). With this choice of sign, if Eq. (22b) is substituted into Eq. (17) and the result is expanded binomially, we obtain the following expression for travel time in terms of receiver time t:

$$T(N,t) = t + (\alpha_1 - t)(1+\alpha_2)^{-1} + \alpha_3(\alpha_1-t)^2(1+\alpha_2)^{-3} \quad . \tag{23}$$

Also, using Snell's law and Eqs. (7b) and (12), we have confirmed that

$$\hat{L}_s^{-1/2}(N,\hat{t}) = L_o^{-1/2}(N)[1 + O(M)] \ , \tag{24}$$

where

$$L_o(N) = R_o^2 \tan^2\theta_{bo} \csc\theta_{bo} \csc\theta_{mo} \tag{25}$$

is the spreading loss for the Nth ray with the source and receiver fixed in a stationary medium.

For the ranges being considered in this paper, it is reasonable to assume that the loss at each bottom reflection of a ray is constant and that the corresponding phase shift is zero.[17,18] Denoting the constant bottom loss by B_o, and keeping only corrections in amplitude larger than O(M), we may now write the following expressions for the amplitude and phase of the Nth ray:

$$A(N,t) = A(N)[1 + O(M)] \doteq L_o^{-1/2}(N) B_o^N \tag{26a}$$

and

$$\phi(N,t) \doteq \omega T(N,t) - (N-1)\pi \quad , \tag{26b}$$

where $T(N,t)$ and $L_o(N)$ are given by Eqs. (23) and (25), respectively. The approximate total acoustic field is now known from Eqs. (10) and (11).

The validity of the expansions in this section and our rationale for retaining second-degree terms in $\hat{t}$ may be explained by examining

$$\hat{\phi}(N,\hat{t}) \doteq [\omega\alpha_1 - (N-1)\pi] + \omega\alpha_2 t + \omega\alpha_3 t^2 \quad . \tag{27}$$

Equation (27) represents the phase of the ray with N bottom reflections in terms of source time $\hat{t}$ and follows from Eqs. (17) and (8b). Since ω is typically 10^3 rad sec^{-1} and assuming that M may be as large as 10^{-2}, it can be shown that if $|\hat{t}| \lesssim 5$ sec, the quadratic term $\omega\alpha_3\hat{t}^2$ is small and $\hat{\phi}(N,\hat{t})$ may be approximated linearly. For larger values of $|\hat{t}|$, $\omega\alpha_3\hat{t}_2$ is larger than M and must be included in the approximation of $\hat{\phi}$(Eq. (27)). To determine the time interval for which Eq. (27) is valid to within a correction of O(M), we derived the cubic term $\omega\alpha_4\hat{t}^3$. We demonstrated that its magnitude remains sufficiently small to assure the validity of Eq. (27) if $|\hat{t}|$ is $\lesssim$ 50 sec at R_o = 5 km and for "large" relative speeds, although bigger time intervals may be justified at longer ranges and more moderate speeds. Thus, second-degree approximations improve the time interval for which our expansions remain valid while avoiding the inherent difficulties of higher

than second-degree equations.

Although the previous paragraphs are concerned with restrictions on $\hat{t}$, corresponding limits on receiver time t may be deduced from Eq. (2a) (appropriately replacing $\hat{T}^*(N,\hat{t})$ with $\hat{T}(N,\hat{t})$) and the fact that at short ranges the ray with one bottom reflection always exists. In particular, the difference between any estimates of the upper limits of $\hat{t}$ and t is the travel time for the N = 1 ray, which can be shown to be less than 10 sec for the ranges considered in this paper. Therefore, the upper bound on t is slightly larger than for $\hat{t}$, but the discussion of restrictions on $\hat{t}$ is essentially valid for t, the time variable of primary interest.

III. NUMERICAL RESULTS AND ANALYTICAL MODEL

Using Eqs. (9b) - (11) and (24), we have obtained numerical results which demonstrate the effects on total-field amplitude and phase of the variation of initial range R_o, receiver speed v_1, source speed v_2, and initial orientations represented by the angles λ_o and ψ_o. At short ranges, the inclination angle of a ray at a bottom reflection is sufficiently large that bottom loss B_o, or ratio of reflected to incident amplitude, remains constant over many ocean areas.[17,18] Therefore, we elected to use the results of Ref. 18 which suggests $B_o = 0.4$ as an appropriate value. Also, we chose the circular frequency at the source to be $\omega = 2\pi f$, where f = 350 Hz, and we fixed the

remaining parameter values as follows:

$g_1 = .0536\ \text{sec}^{-1}$, $g_2 = .0155\ \text{sec}^{-1}$, $c_b = 1522\ \text{m sec}^{-1}$, and $c_m = 1484\ \text{m sec}^{-1}$. We terminated the summations of Eqs. (9b) - (11) at N = N', where N' + 1 denotes the first ray to contribute less than one percent of the amplitude of the N = 1 ray. For all parameter values considered here, the summations could be terminated at N' = 4.

Figure 3 illustrates 60-sec runs for R_o = 2 km and 10 km and for $v_1 = v_2$ = 10 kn ($\doteq 5.14\ \text{m sec}^{-1}$). The sound source $\mathcal{S}$ and receiver $\mathcal{R}$ move on the same linear path, but in opposite directions. Therefore, v = 20 kn ($\doteq 10.28\ \text{m sec}^{-1}$), $\lambda_o = \pi$ rad, and $\psi_o = 0$ rad. Although we show typical 60-sec runs, for these particular receiver and source speeds and directions, results based on approximations such as Eq. (23) remain valid for approximately two minutes of receiver time at R_o = 2 km, and as discussed earlier, for longer periods of time at R_o = 10 km. It can be seen from Fig. 3 that total-field amplitudes show a pseudo-sinusoidal behavior in which both their extent and rate of variation (oscillations per sec) are greater at initial range R_o = 10 km. The total-field cumulative phase shows an overall parabolic behavior in which $0 < \Phi''(t) \ll 1$. To demonstrate this subtle curvature, we have added dashed straight lines tangent to the actual cumulative phase curves at t = 0. Fig. 3 illustrates also that this parabolic behavior becomes more pronounced as R_o decreases, and at R_o = 2 km, there is as much as an 8-cycle difference between the dashed line and the actual parabolic phase curves. It can also be seen that the variation of

phase over time, or phase rate, increases with range for a given relative velocity v. For example, at R_o = 2 km, the variation is approximately 48 cycles over a 60-sec period, whereas at R_o = 10 km, the variation is over 120 cycles. The cumulative-phase values shown at t = 0 were chosen to be those between zero and one cycle. We add that for runs in which the receiver-source distance decreased with time, the cumulative phase rate was negative, as expected, and its magnitude varied with range similar to that just described for positive phase rate. Also, the parabolic nature of cumulative phase at short ranges seemingly contrasts with the essentially linear behavior of phase at long ranges, illustrated and discussed in Refs. 3 thru 6. However, the long-range assumptions of these studies permitted linear time-dependent approximations of phase for reasonable, but suitably restricted, time intervals. If the restrictions on time in these investigations had been relaxed sufficiently to warrant second-degree approximations, a nonlinear pattern for cumulative phase might also be expected at long ranges for sufficiently long sampling periods. Finally, the extent (3-5dB) and more frequent amplitude fades, in addition to the well-behaved amplitude pattern, at the short ranges in this paper contrasts sharply with the deeper (20-25 dB) and less frequent fades of the more noise-like amplitude pattern which these references have described for longer ranges.

The consistent and well-behaved patterns exhibited by total-field amplitude and phase throughout all numerical results

suggest that it should be possible to obtain approximate analytical expressions to explain the behavior of the total-field, rather than relying on numerical computations for particular sets of parameters. Therefore, we forego displaying additional numerical results and turn to the development of an analytical model. Using Eqs. (13) and (25), it can be shown that $A(N)/A(1)$ is $O(10^{-1})$ for $N = 2,3$ and is $O(10^{-2})$ for $N > 3$. With these magnitudes of relative amplitude, Eq. (10) and basic trigonometric identities can be used to write

$$a(t) \doteq A(1) + \beta(t)\cos[\eta(t)] , \tag{28}$$

where

$$\beta(t) = \{[A(2)]^2 + [A(3)]^2 + 2A(2)A(3)\cos[\omega T(3,t)-\omega T(2,t)]\}^{1/2}, \tag{29a}$$

and

$$\eta(t) = \omega[T(2,t)-T(1,t)] + \tan^{-1}\{A(3)\sin[\omega T(3,t)-\omega T(2,t)]\} \times \{A(2) + A(3)\cos[\omega T(3,t)-\omega T(2,t)]\}^{-1} , \tag{29b}$$

where $T(N,t)$ is known from Eq. (23) and $A(N)$ from Eq. (26a).

To approximate $\Phi(t)$, we proceed in a manner somewhat similar to derivations contained in Ref. 19. Specifically, if $\Delta a(t)$ and $\Delta\Phi(t)$ represent the total-field deviations due to motion, then

$$\Delta a(t) = a(t) - a_o \tag{30a}$$

and

$$\Delta\Phi(t) = \Phi(t) - \Phi_o , \tag{30b}$$

where a_o and Φ_o are total-field amplitude and phase, respectively, without receiver and source motion. Using Eqs. (30), Eq. (9b) can be written as the imaginary part of

$$(a_o+\Delta a)\exp\{i[\omega t-\Phi_o-\Delta\Phi]\} = \sum_N A(N)\exp\{i[\omega t-\phi(N,t)]\} \quad . \qquad (31)$$

If both sides of Eq. (31) are multiplied by $\exp\{-i[\omega t - \Phi_o]\}$, and the terms of the summation on the right are combined using basic trigonometric identities, it can be shown that

$$\Phi(t) \doteq \omega T(1,t) + [A(1)]^{-1}\beta(t)\sin[\eta(t)] \quad , \qquad (32)$$

where we drop terms of size less than 10^{-2}, $\Delta a/a_o \ll 1$, and A(N)/A(1) diminishes with N, as discussed previously.

Comparisons of the numerical results obtained from Eqs. (9b) - (11) and (26), and the analytical approximations represented by Eqs. (28) and (32), show that Eq. (28) consistently approximates $a(t)$ to within 0.5 dB, and Eq. (32) approximates $\Phi(t)$ to within 0.05 cycles. In all cases, receiver time was restricted according to initial range and relative speed, as previously discussed. For plotting purposes now and to simplify subsequent analyses, the right side of Eq. (32) may be approximated by

$$\phi(N,t) = \omega[t+(\alpha_1-t)(1+\alpha_2)^{-1} + \alpha_3(\alpha_1-t)^2(1+\alpha_2)^{-3}]-(N-1)\pi \qquad (33)$$

evaluated at N=1, where Eq. (33) follows from substituting Eq. (23) into Eq. (26b). Figure 4 compares numerical and analytical values for a magnified portion of the numerical results in Fig. 3. The results shown are representative of the entire 60-sec run. The

solid curves are numerical results, the dashed amplitude curves are graphs of Eq. (28), and the dashed cumulative phase curves depict Eq. (33) evaluated at N=1. The approximate phase values corresponding to the complete Eq. (32), which contains multipath contributions, generally fall between the solid and dashed phase curves of Fig. 4. Thus, cumulative phase may be conveniently described as the sum of the dominant phase of the N=1 ray, approximated by Eq. (33), and a multipath correction due to the combined contributions of the rays corresponding to $N \geq 2$. This correction, approximated by the second term of the right side of Eq. (32), causes the total-field phase to oscillate subtly about the phase of the N=1 ray. This tendency, confirmed analytically here, was observed also in the computer simulations in Ref. 3. Finally, in contrast to the excellent single-ray approximation to cumulative phase, Eq. (28) shows that the approximation to total-field amplitude relies on the effects of multipath.

IV. TOTAL-FIELD STUDY

We turn next to an examination of the total field using the analytical model developed in Sec. III. This section consists of quantitative descriptions of effects of the variation of initial range and changes in the parameters of motion on total-field amplitude and phase. For brevity, we have omitted other results which could be obtained from Eqs. (28) and (32). As examples, it is possible to describe the relationship between amplitude

oscillations and cumulative phase, as well as to show that the extent of amplitude fades increases with range but is independent of a nonzero relative speed.

For purposes of discussion, we group the effects of receiver and source motion into two categories. The first category consists of effects attributable to the relative motion between the receiver and source, represented by terms containing the parameter M (or equivalently, v). If the receiver is stationary, only this category exists and the relative-motion parameters are determined completely from those of source motion. However, if the receiver is in motion, there is a second category of effects due to an apparent current, represented by terms containing the parameter M_c (or $v_c = v_1$). Furthermore, since a moving receiver also affects relative motion (see Eqs. (3c) and (3d)), receiver-motion contributions to the total field are included in both of the groups just described. Only the second category (current effects) is considered now, while that dealing with relative motion will be addressed subsequently.

As demonstrated earlier, Eq. (33) evaluated at N=1 closely approximates total-field cumulative phase. If Eqs. (18), (19a), and (20a) are substituted into Eq. (33) and if we ignore the small terms for which the sum of the exponents of M and M_c exceeds two, then

$$\Phi \doteq \omega\{T_o(N)[1-M_c \cos\theta_{bo}\cos\lambda_o - MG_2 c_b R_o^{-1}\cos\psi_o]$$

$$+ [M_c MG_1 c_b R_o^{-1} + MG_2 c_b R_o^{-1}\cos\psi_o]t$$

$$+ M^2 H(c_b R_o^{-1})^2 t^2\}\Big|_{N=1} , \qquad (34)$$

where G_1, G_2, and H are given by Eqs. (19b), (19c), and (20), respectively. We have demonstrated numerically that Eq. (34), although simpler than Eq. (33), is an excellent approximation for total-field phase. We have also shown that $G_1 c_b R_o^{-1}$ is O(1), and $G_2 c_b R_o^{-1}$ is $O(10^{-1})$ for $R_o \lesssim 3$ km and O(1) for $3 \lesssim R_o \lesssim 10$ km. Also, $H(c_b R_o^{-1})^2$ increases from approximately 10^{-2} sec^{-1} to $10^{-1} sec^{-1}$ as R_o decreases from 10 km to 2 km. Thus, Eq. (34) shows that current contributions, or second-category effects, are greater than M for both the time-independent and time-dependent portions of total-field phase. Also, in certain cases, these effects dominate those of relative motion. In particular, for $\omega \doteq 10^3$ rad sec^{-1}, the time-independent current effect represented by $\omega_o T_o(1) M_c \cos\theta_{bo}\cos\lambda_o$ ranges from approximately one to ten radians, depending on range, for $\cos\lambda_o$ not close to zero. Suppose, also, that the component of relative velocity $v\cos\psi_o$ is close to zero; i.e., either the path of source motion is essentially perpendicular to the receiver-source line or relative speed is negligible. Then the time-independent current contribution dominates that of relative motion, represented by

the term $\omega T_o(1) M G_2 c_b R_o^{-1} \cos \psi_o$. If $\cos \lambda_o$ is close to zero, however, the current is approximately perpendicular to ray-path planes, and its effects are obviously minimal. Similarly, Eq. (34) shows that for most receiver and source directions, the time-dependent current contribution, represented by the term $\omega M_c M G_1 c_b R_o^{-1} t$, is small in comparison to the time-dependent effects of relative motion. However, it is easy to show that the variation of total-field phase due to current can be as much as 200^o over a two-minute time period for receiver and source speeds of approximately 10 kn and source frequency of 10^3 rad sec^{-1}. Thus, if either the path of relative motion is virtually perpendicular to receiver-source direction or relative speed is negligible, the time dependence of total-field phase can be attributed, within our approximations, to current effects.

In order to simplify our analysis of effects described earlier as belonging to the first category (relative motion effects), we introduce a time-independent approximation to phase rate Φ'. Using Eqs. (19a) and (34), we may approximate with the N=1 ray as follows:

$$\begin{aligned}\dot{\Phi} &\doteq \omega G_2 c_b R_o^{-1} M \cos \psi_o \\ &= \omega \Big(\cos\theta_{bo} \csc\theta_{mo} [\sin\theta_{mo} - \sin\theta_{bo}] [2(g_1^{-1}+g_2^{-1})] \\ &\quad \times \{ (g_1^{-1}+g_2^{-1})(c_b^2 - c_m^2)(c_b R_o^{-1}) + R_o / [4(g_1^{-1}+g_2^{-1}) c_b] \} \Big) \\ &\quad \times R_o^{-1} v \cos \psi_o \,, \end{aligned} \tag{35}$$

where, based on previous discussions of coefficient magnitudes, we have ignored the $M_c Mt$ and $M^2 t$ terms. We remark that the approximation for Φ' could be improved, for example, by using an average over time, or possibly other procedures. For simplicity, we proceed using Eq. (35), which can be used to demonstrate effects of relative motion on total-field amplitude and phase over limited time intervals. We note also that since $\Phi(t)$ generally is not proportional to time, the concept of frequency is not well defined; however, our time-independent approximation of Φ' may be interpreted as an estimate of Doppler-shift frequency with units of rad sec^{-1}.[6,20]

In Fig. 5, the straight lines (solid for R_o = 2 km and 10 km, and dashed for 5 km) follow from Eq. (35). They show effects for different ranges of changes in the component of relative speed in the initial receiver-source direction, $v|\cos\psi_o|$, on a normalized phase rate $\omega^{-1}\Phi'$. Figure 5 illustrates that the effect on phase rate of differences in relative speed is reduced as initial range R_o decreases, and that for a given component of relative speed, differences in range correspond to smaller differences in phase rate at longer ranges. This suggests that as range increases beyond the approximate 10 km limit in this paper, effects of range differences are reduced, and differences in the relative-speed component become the dominant factor in determining phase rate. Finally, as expected, phase rate is positive (negative) according to receiver-source distance increasing (decreasing)

with time, or equivalently, $v\cos\psi_o$ being positive (negative). Moreover, if $v\cos\psi_o = 0$, then the effects of relative motion on phase rate are negligible, although current effects may cause phase to exhibit some time dependence, as discussed earlier. To demonstrate the usefulness of Eq. (35) as an estimate of phase rate for a specified time interval, if $\omega = 2\pi(350)$ rad $\sec^{-1}$ and $v\cos\psi_o = 2$ kn ($\doteq 10.28$ m $\sec^{-1}$), then from Fig. 5 at $R_o = 2$ km, $\phi' \doteq (2.042)\omega \cdot 10^3 = 0.72$ Hz. This value compares favorably with the phase rate of 0.80 Hz, shown in the numerical results of Fig. 3 as a total change in phase of approximately 48 cycles over a 60-sec time period.

Equations (28) and (29) can be used to describe how the time between successive amplitude peaks, which we denote by μ, varies with relative motion at different ranges. In particular, Eq. (28) shows that $a(t)$ reaches a relative maximum with $\beta(t)\cos[\eta(t)]$. Also, Eq. (29b) indicates $\eta(t) \doteq \phi(2,t) - \phi(1,t)$, since $A(3)/A(1)$ is $O(10^{-1})$ and therefore, $\cos[\eta(t)]$ peaks when $\cos[\phi(2,t) - \phi(1,t)] \doteq 1.0$. Approximating $\beta(t)$ with $A(2)$, we conclude that $\beta(t)\cos[\eta(t)]$ peaks at approximately the same time as $A(2)\cos[\phi(2,t) - \phi(1,t)]$. Also, if $\phi'(2,t)$ is approximated linearly in the same manner as $\phi'(1,t)$ in Eq. (35), we obtain

$$\eta(t) \doteq \phi(2,t)-\phi(1,t) \doteq \omega[G_2(2)-G_2(1)]R_o v(\cos\psi_o)t+K \ , \qquad (36)$$

where K is a constant. From Eq. (36), it follows that

$$\mu \doteq |f[G_2(2)-G_2(1)]R_o^{-1}v\cos\psi_o|^{-1} \ , \qquad (37)$$

where f is frequency in Hz. Equation (37) provides a simple expression with which to analyze the effects on μ of changes in relative-speed component and range. The hyperbolas in Fig. 5 illustrate such effects for a normalized peak-to-peak time μf at R_o = 2 km and 10 km (solid curves) and at an intermediate range of 5 km (dashed curve). In contrast to phase rate, which essentially increases or decreases proportionally to $v\cos\psi_o$, differences in peak-to-peak time μf corresponding to differences in relative-speed component are much greater at lower than at higher speeds. Also, for a particular value of $v|\cos\psi_o|$, a change in range corresponds to a greater change in μf at lower speeds; and similar to the variation in phase rate, differences in range correspond to smaller differences in μf at longer ranges. As expected, if $v|\cos\psi_o|$ is small, μf becomes large, consistent with amplitude becoming constant over time as relative motion becomes negligible. In addition, the results using Eq. (37) and shown in Fig. 5 agree favorably with numerical results. For example, if v = 20 kn ($\doteq$ 10.28 m sec^{-1}), R_o = 2 km, f = 350 Hz, and $\cos\psi_o$ = 1, then from Fig. 5, $\mu \doteq$ 2.86 sec. For the 60-sec run in Fig. 3 there are approximately 23 fades in 60 sec for an average time between amplitude peaks of 2.61 sec. Figure 5 suggests also that for a given relative-speed component, the time between amplitude peaks achieves a relative minimum in the interval 2 km < R_o < 5 km. This can be confirmed analytically, although not included here, by showing that $R^{-1}|G_2(2)-G_2(1)|$, as

a function of initial range R_o, has a relative maximum in the same interval.

As noted earlier, acoustical effects of a moving receiver can be classified as those due to a uniform current, already discussed, and those resulting from changes to relative receiver-source motion. In order to consider the latter, it is necessary to examine first the relative-motion parameters as functions of receiver-motion. In the trivial case of a fixed source ($v_2 = 0$), receiver motion completely determines the relative motion and the effects are as described in the preceding paragraphs. If $v_2 \neq 0$, the effects of a moving receiver on relative motion can be portrayed as in Figs. 6(a) and 6(b), using Eqs. (3c) and (3d), respectively. Figure 6(a) shows the effect of changes in a dimensionless receiver speed v_1/v_2 on a dimensionless relative speed v/v_2, while Fig. 6(b) shows the effects of changes in v_1/v_2 on $\cos\psi_o$. For each figure, the directions of source and receiver motion at time t=0 are represented in the term $\cos(\lambda_o-\gamma_o)$, whose values generate a family of curves describing the possible relationships illustrated. Only the solid portions of the parabolas in Fig. 6(a) are valid, since speeds are nonnegative. It can be seen that for $\cos(\lambda_o-\gamma_o) \leq 0$, v/v_2 increases with v_1/v_2 and $\text{sgn}[\cos\psi_o]$ is independent of v_1/v_2. However, if $\cos(\lambda_o-\gamma_o) > 0$, v/v_2 decreases before increasing with v_1/v_2 and $\text{sgn}[\cos\psi_o]$ depends on v_1/v_2. In addition, for Fig. 6(b), if $\cos(\lambda_o-\gamma_o) \neq \pm 1$, there are two possible curves

corresponding to $\cos\psi_o > 0$ and $\cos\psi_o < 0$, respectively; i.e., the relative motion of the source at t=0 may be either away from or toward the receiver. Finally, there are two possibilities each for $\cos(\lambda_o-\gamma_o) = \pm 1$. If $\cos(\lambda_o-\gamma_o)=-1$, then $\cos\gamma_o = +1(-1)$ for all v_1/v_2, if $\cos\gamma_o = +1(-1)$; i.e., receiver-source distance is increasing (decreasing) with time. However, if $\cos(\lambda_o-\gamma_o) = 1$ and $\cos\gamma_o = 1$, then $\cos\psi_o$ jumps from +1 to -1 at $v_1/v_2 = 1$; if $\cos\gamma_o = -1$, $\cos\psi_o$ jumps from -1 to +1 at $v_1/v_2 = 1$. Thus, v_1/v_2 determines the sign of the rate of change of receiver-source distance as was the case for $\cos(\lambda_o-\gamma_o) > 0$.

Equations (3c) and (3d) can be substituted into Eqs. (35) and (37) in order to examine specifically the effects of receiver motion on total-field amplitude and phase for a particular source speed and range. As an illustration, we show such effects for v_2 = 20 kn ($\doteq$ 10.28 m $\sec^{-1}$) and R_o = 2 km in Figs. 7 and 8. It can be seen from Fig. 7 that for nonpositive values of $\cos(\lambda_o-\gamma_o)$, since the time rate of change of receiver-source distance does not change sign and either increases or decreases with v_1, the correspondence between $\omega^{-1}\Phi'$ and receiver speed is straightforward and virtually linear. However, if $\cos(\lambda_o-\gamma_o) > 0$, differences in $\omega^{-1}\Phi'$ due to differences in receiver speed depend greatly on the magnitude of v_1, including a possible difference in sign. For example, if $\cos(\lambda_o-\gamma_o) = 1/2$ and the source is moving away from the receiver, there is an approximate difference

of 1.0 in $10^3\omega^{-1}\Phi'$ corresponding to the two values $v_1/v_2 = 0$ and 0.5. However, if the relative speed is between 0.5 and 1.5, the corresponding difference in $10^3\omega^{-1}\Phi'$ is small; if v_1/v_2 exceeds 2.0, $10^3\omega^{-1}\Phi'$ is negative. This pattern of behavior of $\omega^{-1}\Phi'$ is a direct result of the earlier discussions regarding the effects of changes in receiver speed v_1 on both v and $\cos\psi_o$ when $\cos(\lambda_o-\gamma_o) > 0$, which can be seen in Figs. 6(a) and 6(b) for the same values of v_1/v_2.

Trends for μf are shown in Fig. 8, using the same values of R_o and source speed v_2 as in Fig. 7. As discussed previously, if $\cos(\lambda_o - \gamma_o) < 0$, the time rate of change of receiver-source distance does not change sign, and its magnitude increases with v_1. This is equivalent to $|v\cos\psi_o|$ being bounded away from zero and increasing with v_1. The result is that μf decreases, but at a rate which depends on the receiver and source directions, or on $\cos(\lambda_o - \gamma_o)$. However, if $\cos(\lambda_o - \gamma_o) > 0$, the variation of μf with receiver speed v_1 is less predictable, as was the case for the variation of $\omega^{-1}\Phi'$ with v_1. Also, the tendency of μf to increase without bound corresponds to total-field amplitude becoming constant. This geometric consequence can be attributed to that particular ratio of receiver and source speeds which, for a given combination of receiver and source directions, causes the relative-speed component to become zero and results in a negligible time rate of change of the horizontal distance traveled by the

sound rays. Also from Fig. 8, if the receiver is stationary ($v_1/v_2 = 0$), then $10^{-3}\ \mu f = 1$. Since v_2 = 20 kn ($\doteq$ 10.28 m sec^{-1}) and R_o = 2 km, if f = 350 Hz, then $\mu \doteq 2.87$ sec. This agrees closely with the numerical results of Fig. 3 (discussed earlier) for which both receiver and source were moving, but with the same relative speed of 20 kn. It can be seen from Fig. 8, however, that for $v_1 > 0$, the effects of receiver motion are distinctly different, depending on the receiver and source directions. We note that graphs similar to those in Figs. 7 and 8 could be sketched for other parameter choices, although the trends would remain the same. Also, for smaller values of source speed, the intercepts on the vertical axes decrease for $\omega^{-1}\phi'$ and increase for μf, and conversely for larger values. Such figures illustrate vividly the significant effects on total field which can be caused by differences in receiver speed, depending on receiver and source directions, source speed, and range.

V. SUMMARY

This paper presents an analysis of the effects of source and receiver motion on a CW signal transmitted in a deep-ocean channel over short ranges. The source and receiver each follow constant-velocity horizontal paths on the ocean surface. A bilinear sound-speed profile and horizontal, smooth boundaries are assumed. The moving source, moving receiver problem is transformed into a

geometrically and acoustically equivalent fixed-receiver model. Under certain time restrictions, general equations are derived for the launch angles, travel times, and spreading losses of SRBR rays, which lead to time-dependent total-field phase and amplitude expressions. Because of the short ranges, linear approximations in previous studies are replaced by second-order approximations in order to maintain mathematically valid expressions over time intervals of sufficient length.

Total-field amplitude and cumulative phase are calculated as functions of time for various source/receiver speeds, orientations, and ranges. It is shown that amplitude displays a rapidly oscillating pseudo-sinusoidal behavior and that cumulative phase exhibits an overall parabolic pattern, with a subtle oscillatory behavior on a smaller scale. These results contrast with the more noise-like, but slower oscillating, amplitudes and the essentially linear behavior of cumulative phase over time demonstrated in previous investigations for comparable time intervals but at longer ranges.

Analytical expressions are derived which closely approximate numerical results. These expressions provide the basis for studying total-field amplitude and phase in terms of arbitrary motion parameters and initial range. It is shown that phase rate increases strictly with both range and the component of relative speed in the receiver-source direction, with the effects of changes in range diminishing at larger ranges. Peak-to-peak

amplitude time is shown to decrease with an increase in relative speed, with the effects of changes in speed diminishing at higher speeds and the effects of differences in range diminishing with higher ranges.

The effects of receiver motion on total field are illustrated and discussed. It is demonstrated that a moving receiver contributes to the total field by introducing a current effect and also by changing the relative motion. In general, the primary current contribution is a constant shift in total-field phase, with the dependency of phase on time being dominated by relative motion. However, for certain receiver-source directions, the time-dependent current effect can cause significant variations in total-field phase and the time-dependence of phase may essentially be attributed to only current effects. Significant receiver-motion effects on total field, through changes in relative motion, are demonstrated, to include the relative importance of receiver-source directions, as well as the ratio of receiver speed to source speed.

REFERENCES

[1]R.B. Lindsay, Mechanical Radiation (McGraw-Hill, New York 1960), pp. 311-321.

[2]P.M. Morse and K.U. Ingard, Theoretical Acoustics (McGraw-Hill, New York, 1968), pp. 699-726.

[3]R.P. Flanagan, N.L. Weinberg, and J.G. Clark, J. Acoust. Soc. Am. 56, 1673-1680 (1974).

[4]J.G. Clark, R.P. Flanagan, and N.L. Weinberg, J. Acoust. Soc. Am. 60, 1274-1284 (1976).

[5]G.M. Jacyna, M.J. Jacobson, and J.G. Clark, J. Acoust. Soc. Am. 60, 815-824 (1976).

[6]G.M. Jacyna and M.J. Jacobson, J. Acoust. Soc. Am. 61, 1153-1162 (1977).

[7]J.A. Neubert, J. Acoust. Soc. Am. 62, 1404-1411 (1977).

[8]R.E. Wilcox, J. Acoust. Soc. Am. 63, 870-875 (1978).

[9]G.M. Jacyna and M.J. Jacobson, J. Acoust. Soc. Am. 63, 1353-1364 (1978).

[10]R.J. Urick, Principles of Underwater Sound (McGraw-Hill), New York, 1975, 2d edition), pp. 53-54.

[11]C.B. Officer, Introduction to the Theory of Sound Transmission (McGraw-Hill, New York, 1958), pp. 228-248.

[12]R.N. Baer and M.J. Jacobson, J. Acoust. Soc. Am. 54, 90-91 (1973).

[13]J.A. Widtfeldt and M.J. Jacobson, J. Acoust. Soc. Am. 59, 852-860 (1976).

[14]K.G. Hamilton, W.L. Siegmann, and M.J. Jacobson, J. Acoust. Soc. Am. 62, 53-62 (1977).

[15]L.A. Stallworth and M.J. Jacobson, J. Acoust. Soc. Am. 52, 344-355 (1972).

[16]B.K. Newhall, M.J. Jacobson, and W.L. Siegmann, J. Acoust. Soc. Am. 62, 1165-1175 (1977).

[17]Ref. 10, pp. 126-132.

[18]K.V. Mackenzie, J. Acoust. Soc. Am. 32, 221-231 (1960).

[19]W.L. Siegmann, M.J. Jacobson, K.G. Hamilton, "Effects of Tidally-varying sound-speeds in acoustical propagation over a sloping ocean bottom," Rensselaer Polytechnic Institute, Math. Rep. No. 123, 1 February 1979 (unpublished).

[20]Ref. 2, pp. 717-732.

FIGURE LEGENDS

FIG. 1. (a) Bilinear sound-speed channel and (b) geometry for constant-velocity receiver and source motions.

FIG. 2. Moving reference frame geometry for receiver and source motions shown in Fig. 1.

FIG. 3. Cumulative phase and amplitude vs time over a 60-sec interval for R_o = 2 km and 10 km with $v_1 = v_2$ = 10 kn, $\psi_o = 0$.

FIG. 4. Approximate (dashed) and numerical (solid) cumulative phase and amplitude for portion of run in Fig. 3. Parameter values as in Fig. 3.

FIG. 5. Normalized phase rate ($10^3\omega^{-1}\Phi'$) and normalized peak-to-peak amplitude time ($10^{-3}\mu f$) vs relative-speed component ($v|\cos\psi_o|$) at different initial ranges.

FIG. 6. (a) Dimensionless relative speed (v/v_2) and (b) $\cos\psi_o$ vs dimensionless receiver speed (v_1/v_2) for different receiver and source directions ($\cos(\lambda_o - \gamma_o)$), where $v_2 \neq 0$.

FIG. 7. Normalized phase rate ($\omega^{-1}\Phi'$) vs dimensionless receiver speed (v_1/v_2) for R_o = 2 km, v_2 = 10 kn, and different receiver and source directions ($\cos(\lambda_o - \gamma_o)$).

FIG. 8. Normalized peak-to-peak amplitude time (μf) vs dimensionless receiver speed (v_1/v_2) for R_o = 2 km, v_2 = 10 kn, and different receiver and source directions ($\cos(\lambda_o - \gamma_o)$).

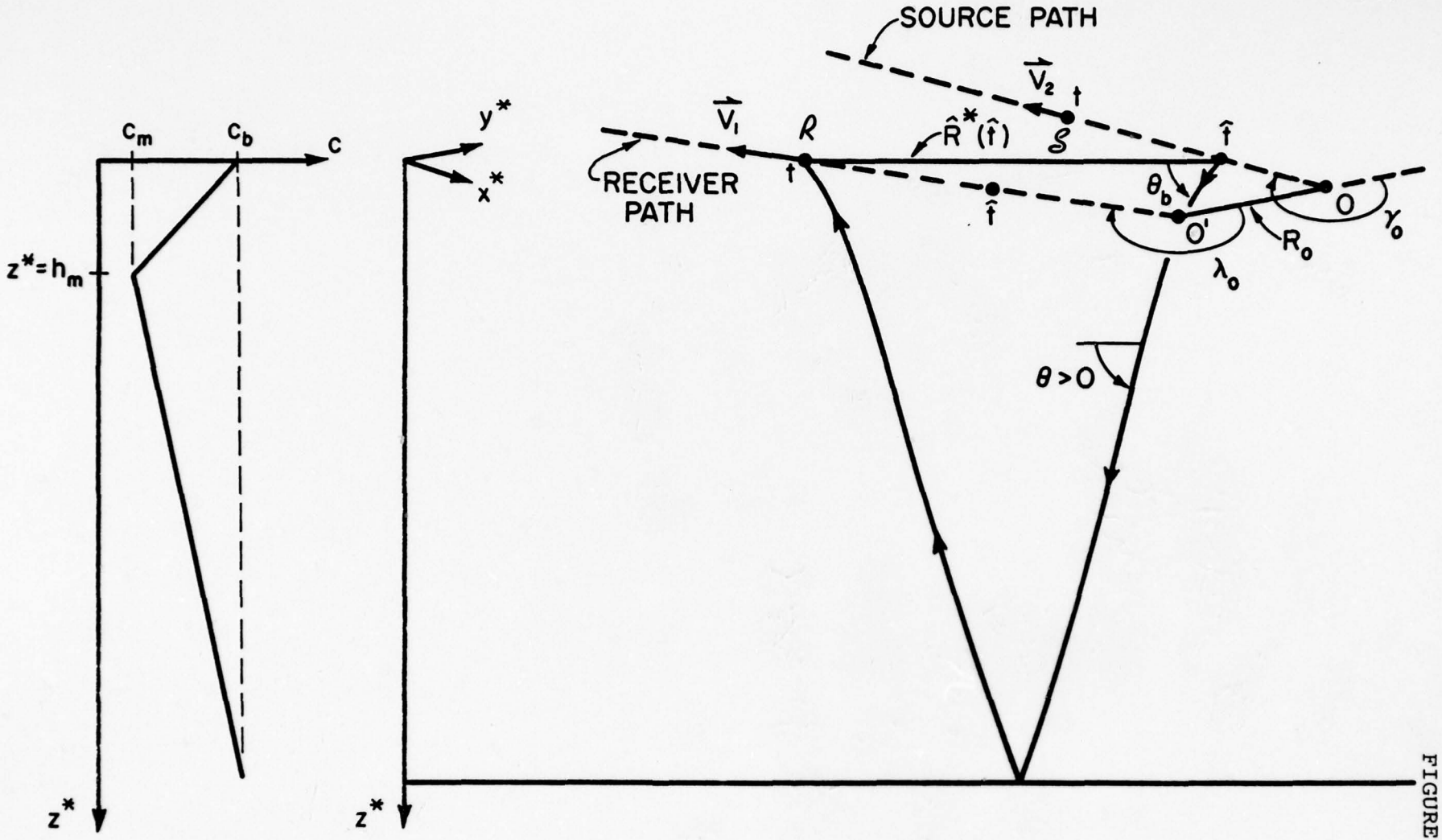
c_m
c_b
c
$z^* = h_m$
z^*
(a)
y^*
x^*
z^*
SOURCE PATH
$\vec{V}_2$
t
$\vec{V}_1$
R
$\hat{R}^*(\hat{t})$
S
$\hat{t}$
RECEIVER PATH
t
$\hat{t}$
θ_b
O
γ_o
O'
R_o
λ_o
$\theta > 0$
(b)

FIGURE 1

FIGURE 2

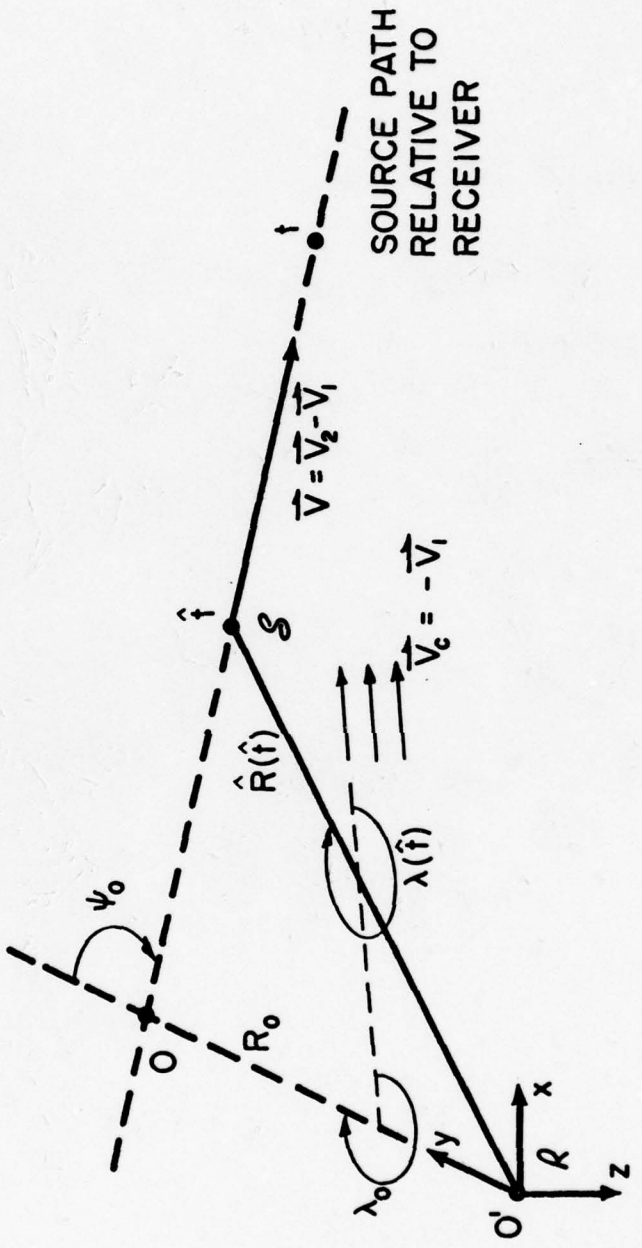
SOURCE PATH
RELATIVE TO
RECEIVER
t
$\vec{V}=\vec{V}_2-\vec{V}_1$
$\hat{t}$
S
$\vec{V}_c=-\vec{V}_1$
$\hat{R}(\hat{t})$
$\lambda(\hat{t})$
ψ_o
O
R_o
λ_o
y
x
z
R
O'

FIGURE 3

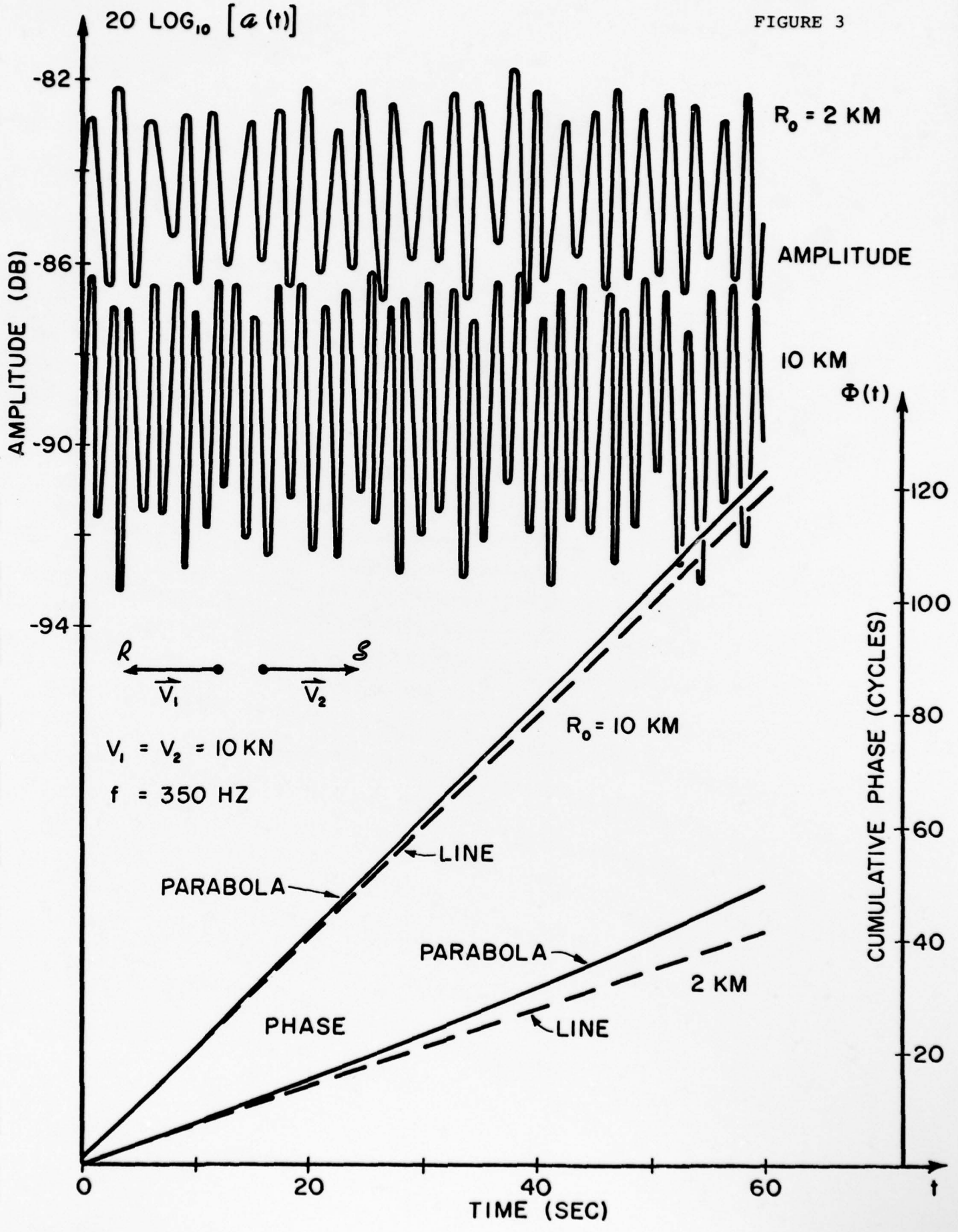
20 LOG10 [a (t)]
-82
-86
-90
-94
AMPLITUDE (DB)
R0 = 2 KM
AMPLITUDE
10 KM
Φ(t)
120
100
80
60
40
20
CUMULATIVE PHASE (CYCLES)
R
S
V1
V2
V1 = V2 = 10 KN
f = 350 HZ
R0 = 10 KM
LINE
PARABOLA
PARABOLA
2 KM
PHASE
LINE
0
20
40
60
t
TIME (SEC)

FIGURE 4

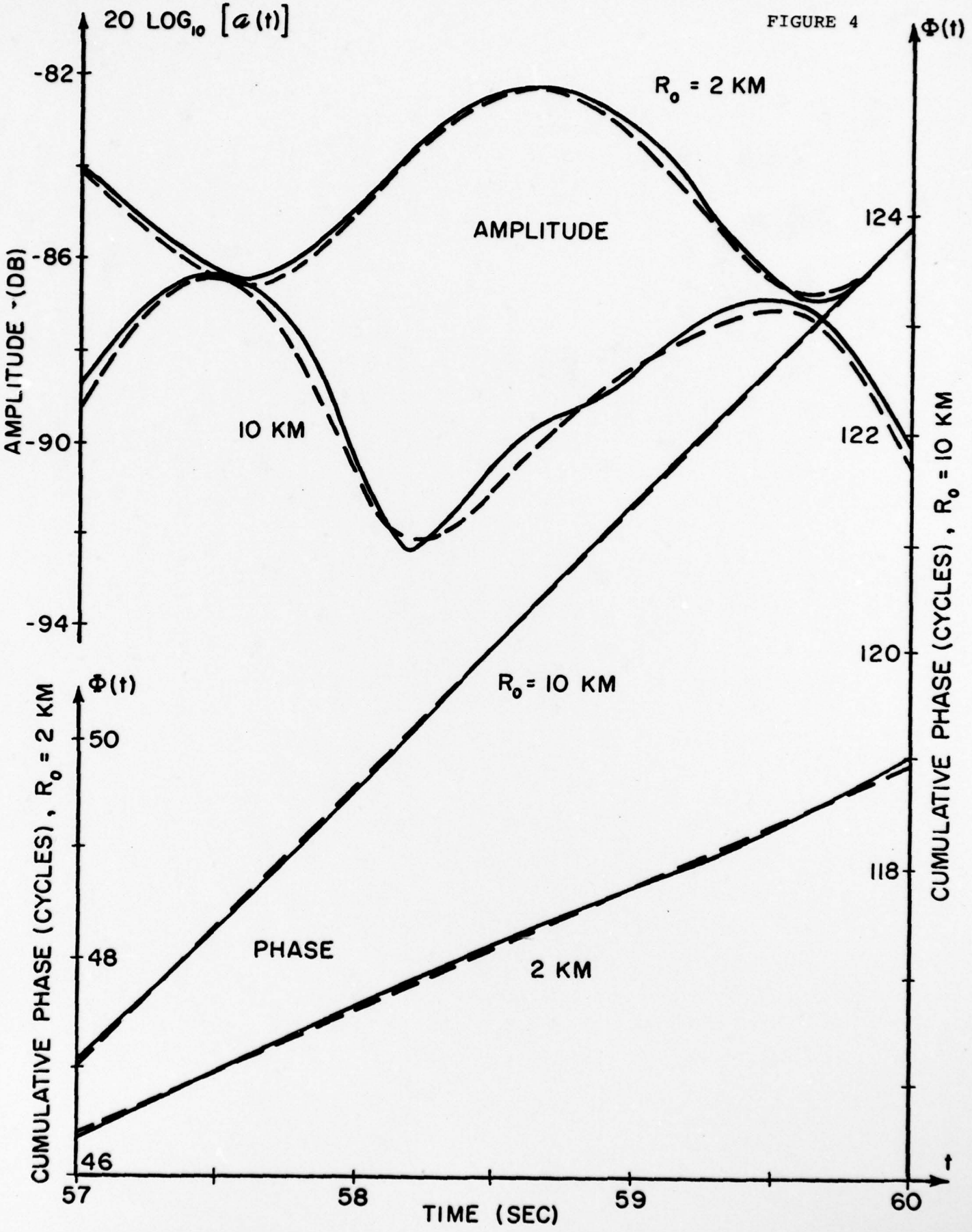
20 LOG10 [a(t)]
Φ(t)
-82
-86
-90
-94
AMPLITUDE -(DB)
R0 = 2 KM
AMPLITUDE
10 KM
124
122
120
118
CUMULATIVE PHASE (CYCLES), R0 = 10 KM
R0 = 10 KM
Φ(t)
50
48
46
CUMULATIVE PHASE (CYCLES), R0 = 2 KM
PHASE
2 KM
57
58
59
60
t
TIME (SEC)

FIGURE 5

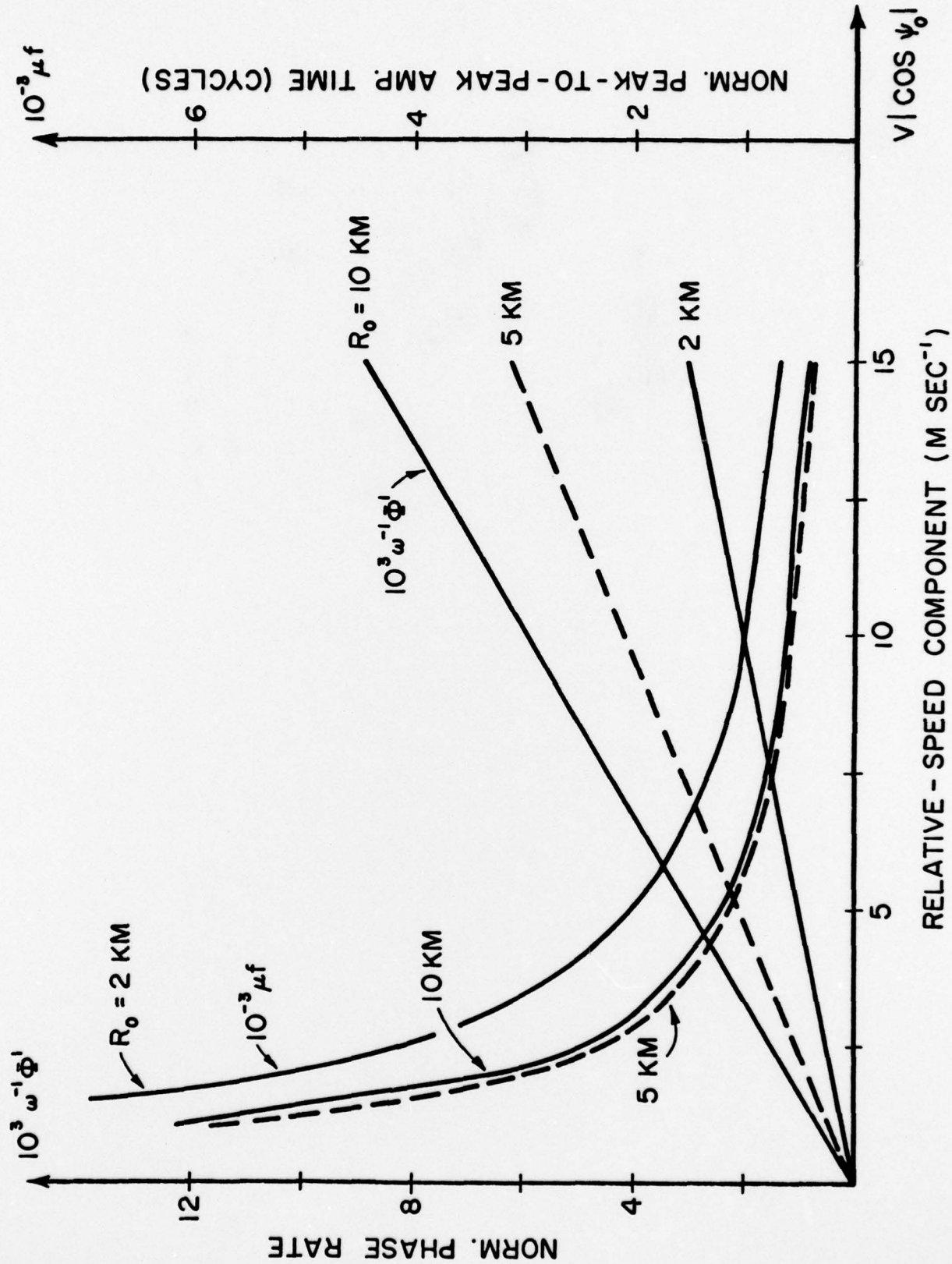
NORM. PHASE RATE
$10^3\,\omega^{-1}\Phi'$
12
8
4
$R_0 = 2$ KM
$10^{-3}\mu f$
10 KM
5 KM
$10^3\omega^{-1}\Phi'$
$R_0 = 10$ KM
5 KM
2 KM
NORM. PEAK-TO-PEAK AMP. TIME (CYCLES)
$10^{-3}\mu f$
6
4
2
RELATIVE-SPEED COMPONENT (M SEC^{-1})
5
10
15
$V|\cos\psi_0|$

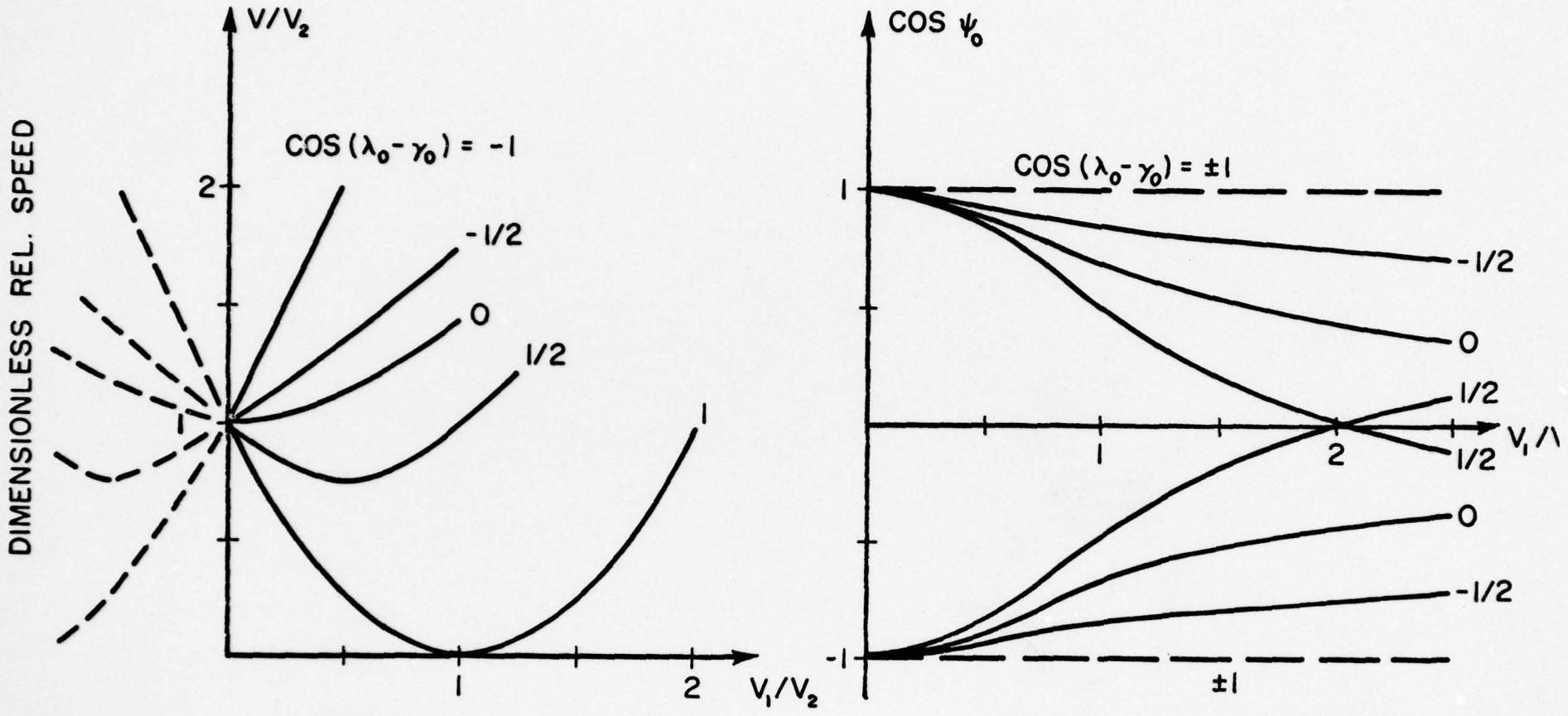
V/V₂
COS (λ₀ - γ₀) = -1
2
-1/2
0
1/2
1
1
2
V₁/V₂
DIMENSIONLESS REL. SPEED
DIMENSIONLESS REC. SPEED
(a)
COS ψ₀
COS (λ₀ - γ₀) = ±1
1
-1/2
0
1/2
1
2
1/2
V₁/V
0
-1/2
-1
±1
DIMENSIONLESS REC. SPEED
(b)

FIGURE 9

FIGURE 7

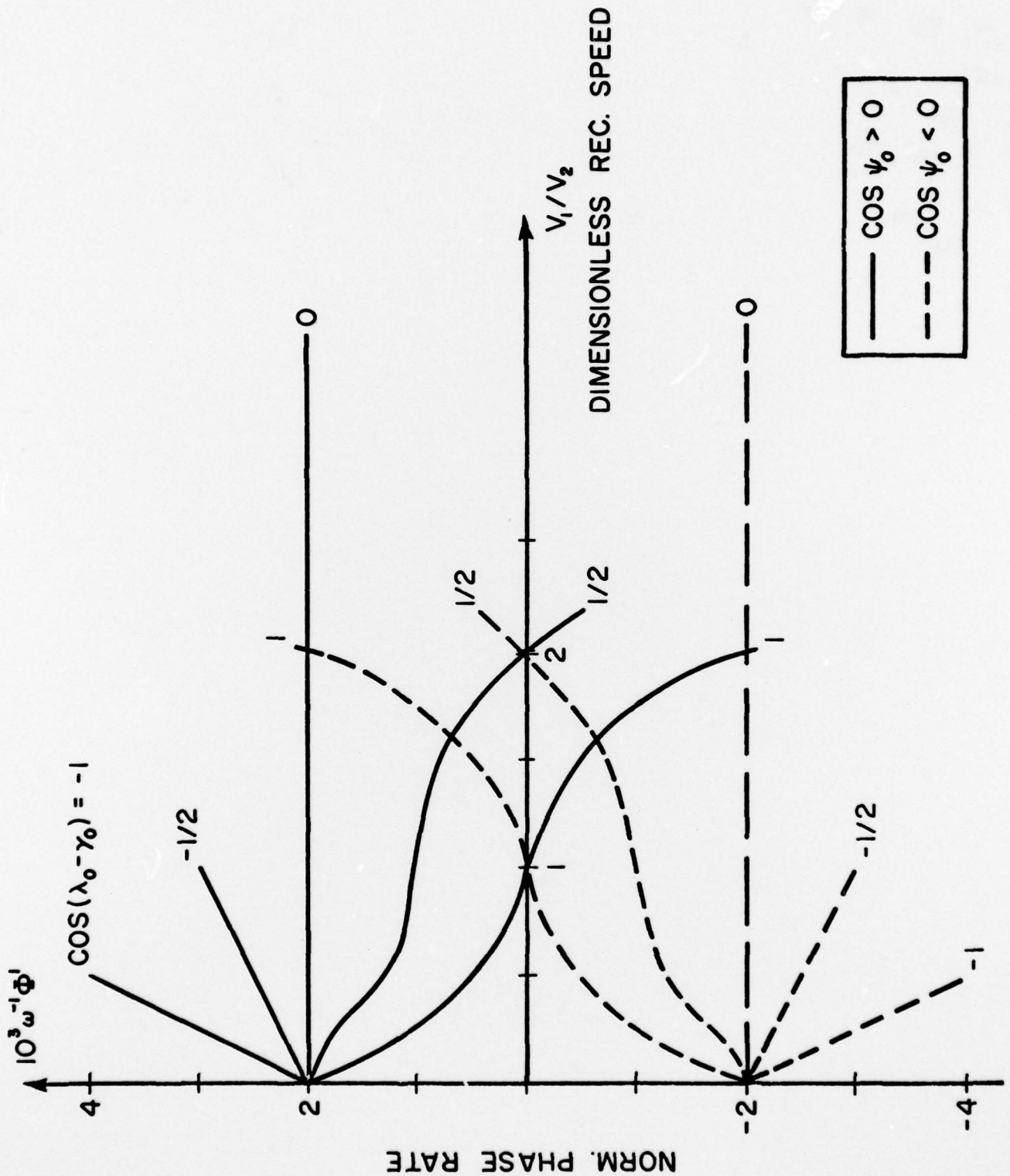
NORM. PHASE RATE
$10^3\omega^{-1}\dot{\Phi}'$
4
2
-2
-4
$\cos(\lambda_0-\gamma_0) = -1$
-1/2
0
1/2
1
2
-1/2
-1
V_1/V_2
DIMENSIONLESS REC. SPEED
$\cos\psi_0 > 0$
$\cos\psi_0 < 0$

FIGURE 8

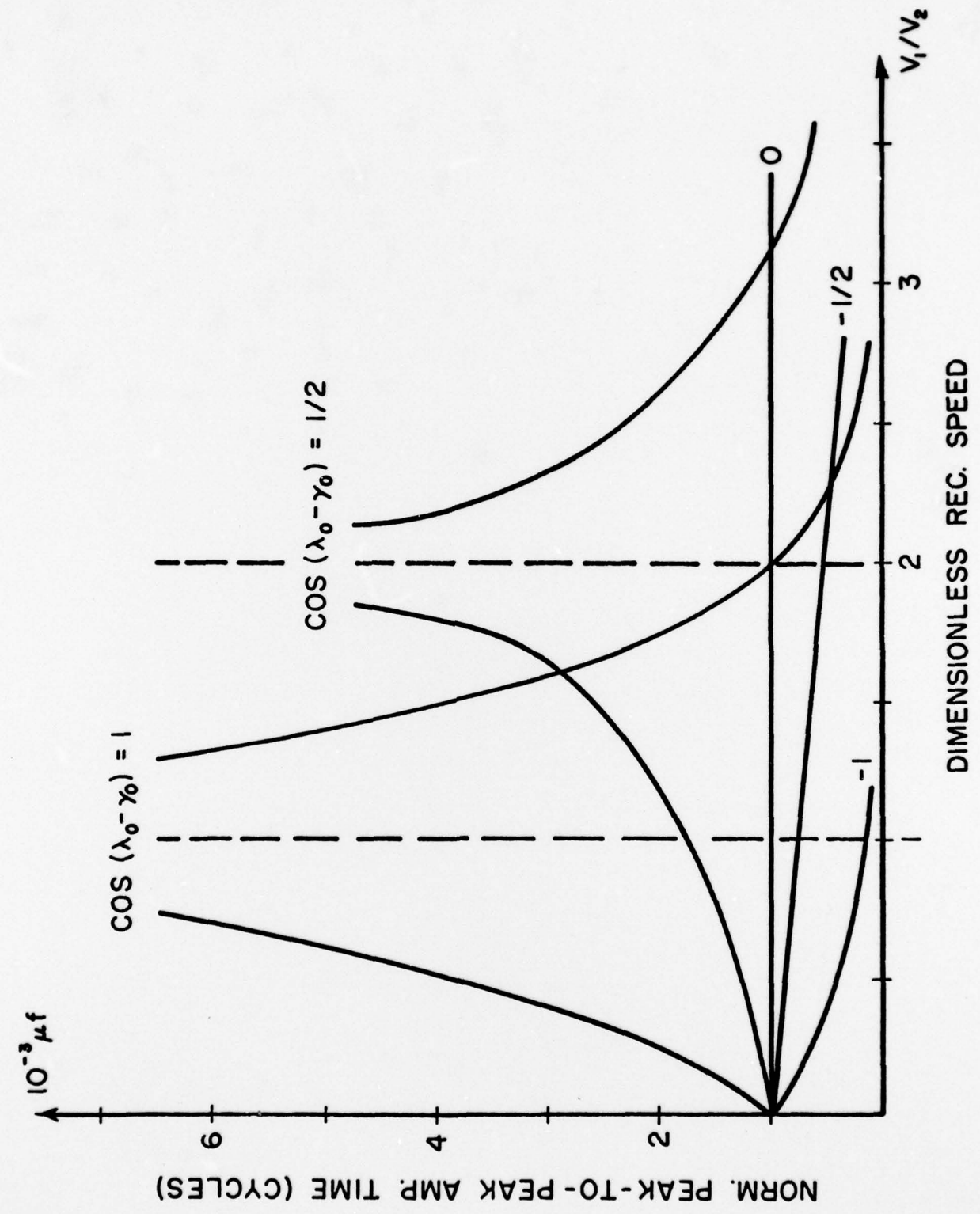
NORM. PEAK-TO-PEAK AMP. TIME (CYCLES)
$10^{-3}\mu f$
2
4
6
$\cos(\lambda_0-\gamma_0) = 1$
$\cos(\lambda_0-\gamma_0) = 1/2$
0
-1/2
-1
1
2
3
V_1/V_2
DIMENSIONLESS REC. SPEED

DISTRIBUTION LIST

Office of Naval Research (Code 222) (Code 102-OS) (Code 480) Department of the Navy Arlington, Virginia 22217		2 1 1
Director Naval Research Laboratory Technical Information Division Washington, D. C. 20375		6
Director Office of Naval Research Branch Office 1030 East Green Street Pasadena, California 91106		1
Office of Naval Research San Francisco Area Office 760 Market Street - Room 447 San Francisco, California 94102		1
Director Office of Naval Research Branch Office 495 Summer Street Boston, Massachusetts 02210		1
Office of Naval Research New York Area Office 207 West 24th Street New York, New York 10011		1
Director Office of Naval Research Branch Office 536 South Clark Street Chicago, Illinois 60605		1
Code 102 IP Office of Naval Research Arlington, Virginia 22217	(Uncl.) (No Class. Reports)	8
Commander Naval Ordnance Laboratory Acoustics Division White Oak Silver Spring, Maryland 20910 ATTN: Dr. Zaka Slawsky		1

DISTRIBUTION LIST - 2

Officer in Charge 1
Annapolis Laboratory
Naval Ship Research and Development Center
Annapolis, Maryland 21402

Commander 1
Naval Sea Systems Command
Code SEA 037
Washington, D. C. 20362

Commander
Naval Sea Systems Command
Washington, D. C. 20362
ATTN: Mr. Carey D. Smith (Code SEA 06H1) 1
CDR Bruce Gilchrist (Code SEA 06H2) 1

Officer in Charge 1
Pasadena Laboratory
Naval Undersea Center
3202 East Foothill Boulevard
Pasadena, California 91107

Commanding Officer 1
Fleet Numerical Weather Central
Monterey, California 93940

Defense Documentation Center 20
Cameron Station
Alexandria, Virginia 22314

Chief of Naval Material 1
Department of the Navy
Washington, D. C. 20360
ATTN: Dr. James Probus (Acting Director
of Navy Laboratories)

Office of the Secretary of Defense 1
OSD
Pentagon, Room 3E1040
Washington, D. C. 20350
ATTN: Mr. Allan D. Simon

Commander
Naval Electronic Systems Command
Washington, D. C. 20360
ATTN: Capt. D. Pajus (NAVELEX 03) 1
CDR A. Miller (NAVELEX 320) 1

DISTRIBUTION LIST - 3

Chief of Naval Operations Department of the Navy Pentagon, Room 5B718 Washington, D. C. 20350 ATTN: CAPT Robert B. Brunsted	1
Commander Naval Ship Research and Development Center Bethesda, Maryland 20034 ATTN: Mr. Craig Olson	1
Chief of Naval Operations Department of the Navy Pentagon, Room 4C559 Washington, D. C. 20350 ATTN: CDR A. H. Gilmore	1
Commander Naval Undersea Center San Diego, California 92132 ATTN: Dr. Dan Andrews Mr. Henry Aurand	 1 1
Chief Scientist Navy Underwater Sound Reference Division P. O. Box 8337 Orlando, Florida 32806	1
Officer in Charge New London Laboratory Naval Underwater Systems Center New London, Connecticut 06320	1
Commander Naval Air Development Center Warminster, Pennsylvania 18974	1
Commander Naval Ship Research and Development Center Bethesda, Maryland 20034	1
Superintendent Naval Postgraduate School Monterey, California 93940	1
Commanding Officer Naval Coastal Systems Laboratory Panama City, Florida 32401	1
Commanding Officer Naval Underwater Systems Center Newport, Rhode Island 02840	1

DISTRIBUTION LIST - 4

Superintendent
Naval Academy
Annapolis, Maryland 21402 — 1

Commanding Officer
Naval Intelligence Support Center
4301 Suitland Road
Washington, D. C. 20390
ATTN: Dr. Johann Martinek — 1
Mr. E. Bissett — 1

Commander
Naval Sea Systems Command
Code SEA 03E
Washington, D. C. 20362 — 1

Dr. Melvin J. Jacobson
Rensselaer Polytechnic Institute
Troy, New York 12181 — 1

Dr. Charles Stutt
General Electric Company
P. O. Box 1088
Schenectady, New York 12301 — 1

Dr. Alan Winder
MSB Systems, Inc.
110-16 72nd Avenue
Forest Hills, New York 11375 — 1

Dr. T. G. Birdsall
Cooley Electronics Laboratory
University of Michigan
Ann Arbor, Michigan 48105 — 1

Dr. Harry DeFerrari
University of Miami
Rosenstiel School of Marine and
Atmospheric Sciences
Miami, Florida 33149 — 1

Mr. Robert Cunningham
Bendix Electronics Center
15825 Roxford Street
Sylmar, California 91342 — 1

Dr. Stephen Wolff
John Hopkins University
Baltimore, Maryland 21218 — 1

DISTRIBUTION LIST - 5

Dr. M. A. Basin
S. D. P., Inc.
15250 Ventura Boulevard, Suite 518
Sherman Oaks, California 91403 — 1

Commanding Officer
New London Laboratory
Naval Underwater Systems Center
New London, Connecticut 06320
ATTN: Dr. Albert Nuttall — 1

Dr. Walter Duing
University of Miami
Rosenstiel School of Marine and
Atmospheric Sciences
Miami, Florida 33149 — 1

Commanding Officer
New London Laboratory
Naval Underwater Systems Center
New London, Connecticut 06320
ATTN: Dr. H. W. Marsh
Dr. D. M. Viccione — 1

Dr. David Middleton
127 East 91st Street
New York, New York 10028 — (Uncl.) 1

Dr. David Middleton
c/o ONR New York Area Office
207 West 24th Street
New York, New York 10011 — (Class.) 1

Dr. Donald W. Tufts
University of Rhode Island
Kingston, Rhode Island 02881 — 1

Dr. Loren W. Nolte
Department of Electrical Engineering FT-10
University of Washington
Seattle, Washington 98195 — 1

Mr. S. W. Autrey
Hughes Aircraft Company
P. O. Box 3310
Fullerton, California 92634 — 1

Dr. Thomas W. Ellis
Texas Instruments, Inc.
13500 North Central Expressway
Dallas, Texas 75231 — 1

DISTRIBUTION LIST - 6

Mr. Robert Swarts — 1
Applied Physics Laboratory
University of Washington
1013 Northeast Fortieth Street
Seattle, Washington 98195

Institute for Acoustical Research — 2
Miami Division of the Palisades
Geophysical Institute
615 S. W. 2nd Avenue
Miami, Florida 33130
ATTN: Mr. M. Kronengold
Dr. J. Clark
Dr. C. Kimball

Mr. Carl Hartdegen — 1
Palisades Geophysical Institute
Sofar Station
FPO New York 09560

Mr. Charles Loda — 1
Institute for Defense Analyses
400 Army-Navy Drive
Arlington, Virginia 22202

Mr. Beaumont Buck — 1
Polar Research Laboratory
123 Santa Barbara Avenue
Santa Barbara, California 93101

Dr. M. Weinstein — 1
Underwater Systems, Inc.
8121 Georgia Avenue
Silver Spring, Maryland 20910

Dr. Thomas G. Kincaid — 1
General Electric Company
P. O. Box 1088
Schenectady, New York 12301

Applied Research Laboratories — 4
The University of Texas at Austin
P. O. Box 4029
Austin, Texas 78712
ATTN: Dr. Lloyd Hampton
Dr. Charles Wood
Dr. T. D. Plemons

Woods Hole Oceanographic Institute — 1
Woods Hole, Massachusetts 02543
ATTN: Dr. Paul McElroy
Mr. R. Porter
Mr. R. Spindel

DISTRIBUTION LIST - 7

Dr. John Bouyoucos 1
Hydroacoustics, Inc.
321 Northland Avenue
P. O. Box 3818
Rochester, New York 14610

Systems Control, Inc. 1
260 Sheridan Avenue
Palo Alto, California 94306
ATTN: Mr. L. Seidman

Atlantic Oceanographic and Meteorological Laboratories 1
15 Rickenbacker Causeway
Miami, Florida 33149
ATTN: Dr. John Proni

Dr. C. N. K. Mooers 1
University of Miami
Rosenstiel School of Marine and
Atmospheric Sciences
10 Rickenbacker Causeway
Miami, Florida 33149

Unclassified

SECURITY CLASSIFICATION OF THIS PAGE (When Data Entered)

REPORT DOCUMENTATION PAGE		READ INSTRUCTIONS BEFORE COMPLETING FORM
1. REPORT NUMBER: RPI-Math Dept. No. -124	2. GOVT ACCESSION NO.	3. RECIPIENT'S CATALOG NUMBER
4. TITLE (and Subtitle): ANALYSIS OF ACOUSTICAL EFFECTS OF RECEIVER AND SOURCE MOTIONS AT SHORT RANGES IN THE DEEP OCEAN,		5. TYPE OF REPORT & PERIOD COVERED: Technical Report, 6. PERFORMING ORG. REPORT NUMBER
7. AUTHOR(s): M.J. Jacobson, W.L. Siegmann, J.L. Kays		8. CONTRACT OR GRANT NUMBER(s): N 00014-76-C-0288
9. PERFORMING ORGANIZATION NAME AND ADDRESS: Rensselaer Polytechnic Institute, Troy, New York 12181		10. PROGRAM ELEMENT, PROJECT, TASK AREA & WORK UNIT NUMBERS: NR 386-606
11. CONTROLLING OFFICE NAME AND ADDRESS: Office of Naval Research, Code 222, Department of the Navy, Arlington, Virginia 22217		12. REPORT DATE: 1 March 1979; 13. NUMBER OF PAGES: 48
14. MONITORING AGENCY NAME & ADDRESS (if different from Controlling Office)		15. SECURITY CLASS. (of this report); 15a. DECLASSIFICATION/DOWNGRADING SCHEDULE

16. DISTRIBUTION STATEMENT (of this Report)

This document has been approved for public release and sale; its distribution is unlimited

17. DISTRIBUTION STATEMENT (of the abstract entered in Block 20, if different from Report)

18. SUPPLEMENTARY NOTES

19. KEY WORDS (Continue on reverse side if necessary and identify by block number)

Underwater Acoustics
Doppler Effects
Moving Sound Sources
Moving Receivers

20. ABSTRACT (Continue on reverse side if necessary and identify by block number)

An analytical approach is used to determine general results for the effects of both receiver and source motions on a CW signal transmitted through a deep ocean channel at short ranges. A bilinear sound-speed profile is used. The receiver and source are restricted to the surface, and only SRBR rays are relevant. Time-dependent expressions for the total-field amplitude and

(over please)

DD FORM 1 JAN 73 1473 EDITION OF 1 NOV 65 IS OBSOLETE S/N 0102-LF-014-6601

Unclassified

SECURITY CLASSIFICATION OF THIS PAGE (When Data Entered)

phase are developed for appropriately limited time intervals, and numerical results are presented. General analytical expressions for the total field are derived and demonstrated to approximate closely numerical results. These expressions provide the basis for a study of the acoustical effects of varying motion parameters and initial range. It is demonstrated that effects of differences in range on total-field phase rate and the time interval between amplitude maxima are significant at short ranges and diminish as range increases. Effects on total-field due to receiver motion are shown to be both significant and widely varying, depending on receiver and source directions and speeds.

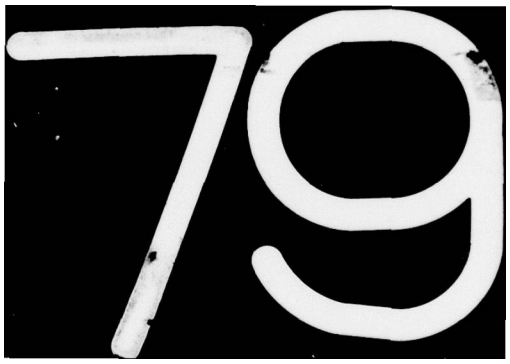
79